ZATTARIN, A., CRUICKSHANK, E., POCIECHA, D., STOREY, J.M.D., GORECKA, E. and IMRIE, C.T. 2024. A design approach to obtaining highly polar liquid crystal dimers. *Liquid crystals* [online], 51(6): a festschrift in honour of Professor Lech Longa, pages 1035-1046. Available from: https://doi.org/10.1080/02678292.2024.2374524

A design approach to obtaining highly polar liquid crystal dimers.

ZATTARIN, A., CRUICKSHANK, E., POCIECHA, D., STOREY, J.M.D., GORECKA, E. and IMRIE, C.T.

2024

Liquid Crystals

ISSN: (Print) (Online) Journal homepage: www.tandfonline.com/journals/tlct20

A design approach to obtaining highly polar liquid crystal dimers

Amerigo Zattarin, Ewan Cruickshank, Damian Pociecha, John M. D. Storey, Ewa Gorecka & Corrie T. Imrie

To cite this article: Amerigo Zattarin, Ewan Cruickshank, Damian Pociecha, John M. D. Storey, Ewa Gorecka & Corrie T. Imrie (2024) A design approach to obtaining highly polar liquid crystal dimers, Liquid Crystals, 51:6, 1035-1046, DOI: 10.1080/02678292.2024.2374524

To link to this article: https://doi.org/10.1080/02678292.2024.2374524

LIQUID CRYSTALS
2024, VOL. 51, NO. 6, 1035–1046
https://doi.org/10.1080/02678292.2024.2374524

A design approach to obtaining highly polar liquid crystal dimers

Amerigo Zattarin[a], Ewan Cruickshank[a*], Damian Pociecha[b], John M. D. Storey[a], Ewa Gorecka[b] and Corrie T. Imrie[a]

[a]Department of Chemistry, School of Natural and Computing Sciences, University of Aberdeen, Aberdeen, UK; [b]Faculty of Chemistry, University of Warsaw, Warsaw, Poland

ABSTRACT

The synthesis and characterisation of 10 members of the [4[(E)-[4-[4-[ω-(4-cyanophenyl)phenoxy]alkyloxy]-3-nitrophenyl]methylideneamino]phenyl] 2,4-dimethoxybenzoates is reported in which the number of methylene units in the flexible spacer is increased from three to twelve. The mesogenic units are based on cyanobiphenyl and 3-nitrobenzylideneaniline benzoate and linked by the spacer such that their dipoles are parallel giving rise to a large longitudinal dipole moment. All 10 members of the series show a nematic phase, and the nematic-isotropic transition temperatures, T_{NI}, and associated entropy changes show a strong dependence on the length and parity of the spacer. This behaviour is attributed to the average shapes of the molecules and their flexibility. The heptyl member was further characterised using dielectric spectroscopy revealing a high value of dielectric permittivity reflecting the large dipole moment of the molecules and possibly indicating local short-range ferroelectric order. The synthesis and characterisation of two members of the [4[(E)-[4-[4-[3-(ω-cyanophenyl)phenoxy]alkyloxy]-4-nitrophenyl]methylideneamino]phenyl] 2,4-dimethoxybenzoates are also described for which the difference in shape between odd and even members is reduced. Both dimers are exclusively nematogenic and the difference between T_{NI} for the odd and even member is smaller reflecting the more similar molecular shapes. The potential for developing dimers that exhibit the ferroelectric nematic phase is discussed.

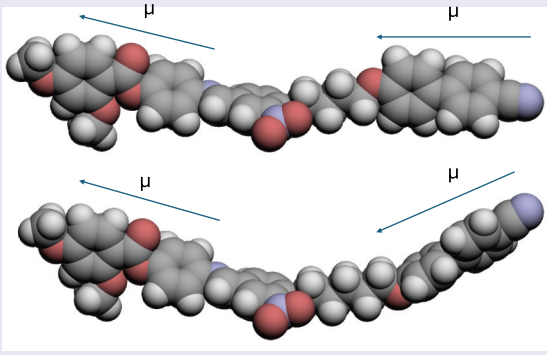

ARTICLE HISTORY
Received 5 April 2024

KEYWORDS
Liquid crystal dimers; odd-even effect; ferroelectric nematic; nematic

1. Introduction

In selecting a theme for our contribution to this Festschrift in honour of Lech Longa we noted his very significant contributions to our understanding of the relationships between molecular shape and phase behaviour. Most recently, these have included probing the role that molecular bend plays in the formation of the twist-bend nematic, N_{TB}, phase [1], and investigating how the shape of tapered molecules stabilises the polar ordering in the ferroelectric nematic, N_F, phase [2]. In this paper, we combine aspects of these general design concepts to develop highly polar liquid crystal dimers to study their potential to exhibit ferroelectric ordering.

Liquid crystal dimers consist of molecules containing two mesogenic units connected by a flexible spacer, most commonly an alkyl chain, and are classed as being symmetric if the two mesogenic moieties are identical and nonsymmetric if they differ [3,4]. Although first reported almost a century ago by

CONTACT Corrie T. Imrie c.t.imrie@abdn.ac.uk
*Present address: School of Pharmacy and Life Sciences, Robert Gordon University, Aberdeen AB10 7GJ, UK.
Supplemental data for this article can be accessed online at https://doi.org/10.1080/02678292.2024.2374524

Vorländer [5], they failed to attract research interest for over 50 years and until the realisation that they could serve as model compounds for the technologically important semi-flexible main chain liquid crystals polymers [6,7]. Subsequently, it became clear that dimers were of considerable interest in their own right and exhibited very different behaviour to that of conventional low molar mesogens consisting of molecules containing a single mesogenic unit attached to which are one or two terminal alkyl chains [8,9]. Dimers have since remained at the forefront of liquid crystal research and their study has resulted in, for example, the discovery of the intercalated smectic phases [10–14], and the twist-bend nematic [15–23] and smectic phases [24–30]. In turn, this research on dimers subsequently triggered considerable interest in higher oligomers including trimers and tetramers [31–36].

It has been reported recently that liquid crystal dimers may also exhibit the ferroelectric nematic phase, N_F [37]. In the conventional uniaxial nematic phase, N, the rod-like molecules lie more or less along a common direction referred to as the director represented by the unit vector **n**. The director has inversion symmetry such that $\mathbf{n} = -\mathbf{n}$, and hence the phase is non-polar. In the N_F phase $\mathbf{n} \neq -\mathbf{n}$ and the phase becomes polar. Around six years ago, a new polar nematic phase was reported [38,39] and later assigned as the N_F phase [40]. There are now a range of structures known to exhibit the N_F phase (see, for example [41–52]). It appears that the essential molecular requirements for the formation of the N_F phase include a large longitudinal dipole moment, some degree of lateral steric bulk and regions of alternating polarity. Rigid and side-chain polymers have also been shown to exhibit the N_F phase [53,54]. The symmetric dimer reported to exhibit the N_F phase consists of benzylideneaniline benzoate moieties, containing fluoro substituents and terminal butyloxy chains, connected by an odd-membered spacer [37]. Although the two mesogenic fragments appear to possess the structural elements required to exhibit the N_F phase, connecting them through a flexible spacer greatly reduces the overall molecular dipole moment. The surprising observation that this dimer exhibited the N_F phase was attributed to a preference for it to adopt U-shaped conformations in which the strong dipole moments associated with the mesogenic units, calculated to be 11.2 D, lie parallel to each other. It is not immediately apparent, however, why such a strong preference for U-shaped conformations should exist for this particular dimer, although the authors suggest that it may arise from the interactions of their strong dipole moments. This report prompted us to consider the design of highly polar liquid crystal dimers. The molecular architecture of a liquid crystal dimer normally ensures that the dipole moments associated with the mesogenic units are orientated in opposing directions. To overcome this, we prepared nonsymmetric dimers, the [4[(E)-[4-[4-[ω-(4-cyanophenyl)phenoxy] alkyloxy]-3-nitrophenyl]methylideneamino]phenyl] 2,4-dimethoxybenzoates, in which the dipole moments of the two mesogenic units are, at least for even-membered homologues, more or less parallel, see Figure 1. We refer to this series using the code **1**-*n* in which *n* refers to the number of methylene units in the spacer, and these dimers are based on a cyanobiphenyl unit and a benzylideneaniline benzoate moiety. In the latter unit, a nitro group is used to give rise to a significant dipole moment, and the 1,3-dimethoxy substitution on the terminal phenyl ring provides the lateral steric bulk thought to be important in the promotion of the N_F phase [55]. By varying the length and parity of the spacer we control the overall molecular shape. In the **1**-*n* series, the two mesogenic units are linked in the *para* position. We have also prepared two examples of the corresponding dimers in which the nitro group on the benzylideneaniline benzoate fragment is in the *para* position and the spacer is connected at the *meta* position, the [4[(E)-[4-[3-[ω-(4-cyanophenyl)phenoxy]alkyloxy]-4-nitrophenyl] methylidene-amino]phenyl] 2,4-dimethoxybenzoates, Figure 2, and these are referred to as **2**-*n*.

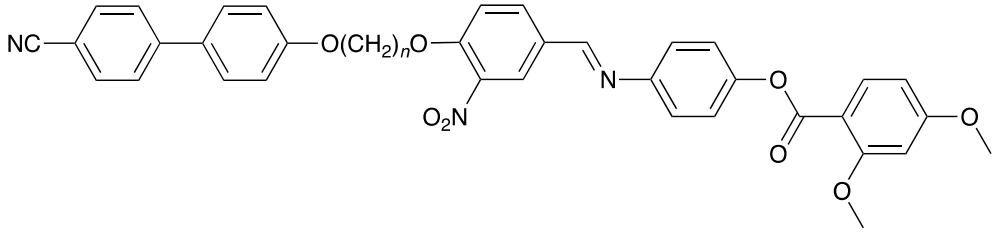

Figure 1. The molecular structure of series **1**-*n* with *n* = 3–12; *n* represents the number of methylene units in the spacer.

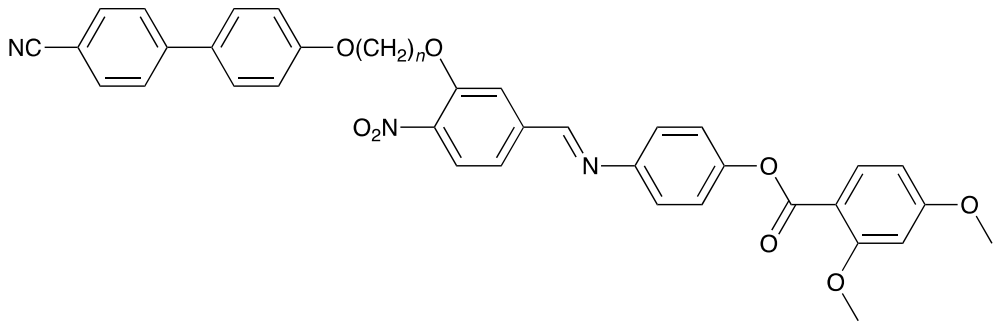

Figure 2. The molecular structure of the **2**-*n* dimers: *n* = 5, 6.

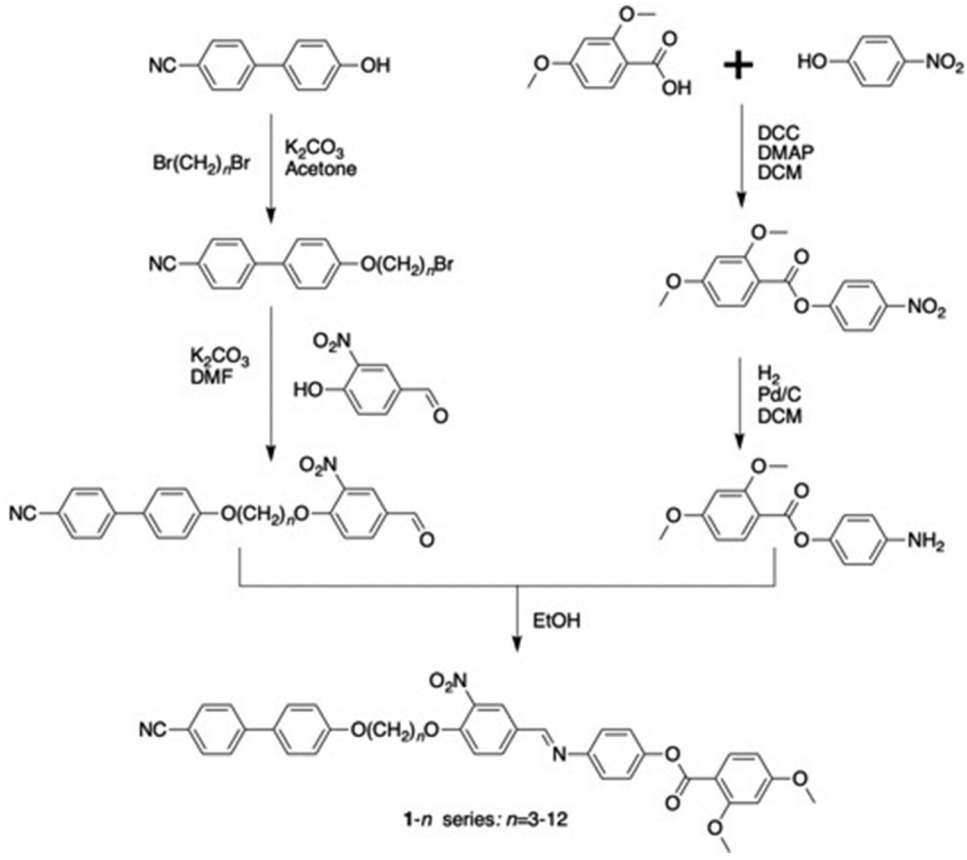

Scheme 1. The preparation of the **1**-*n* series.

2. Experimental

2.1. Synthesis

The synthetic route used to prepare the **1**-*n* series is shown in Scheme 1. The synthesis of the **2**-*n* dimers used essentially the identical route except that 3-hydroxy-4-nitrobenzaldehyde was used in place of 4-hydroxy-3-nitrobenzaldehyde. The preparation of both the **1**-*n* series and the **2**-*n* dimers are described in detail in the Electronic Supplementary Information, and the structural characterisation data for all intermediates and final products is provided.

2.2. Thermal characterisation

The phase behaviour of the new dimers was investigated by differential scanning calorimetry using a Mettler Toledo DSC1 or DSC3 differential scanning calorimeter equipped with TSO 801RO sample robots and calibrated using indium and zinc standards. Heating and cooling rates were 10 K min^{-1}, with a 3-min isotherm between either heating or cooling, and all samples were measured under a nitrogen atmosphere. Transition temperatures and associated enthalpy changes were extracted from the

heating traces unless otherwise noted. Phase characterisation was performed by polarised light microscopy using an Olympus BH2 polarising light microscope equipped with a Linkam TMS 92 hot stage.

2.3. Birefringence measurements

Birefringence was measured with a setup based on a photoelastic modulator (PEM-90, Hinds) working at a modulation frequency f = 50 kHz; as a light source, a halogen lamp (Hamamatsu LC8) was used equipped with narrow bandpass filters (633 nm and 690 nm). The signal from a photodiode (FLC Electronics PIN-20) was deconvoluted with a lock-in amplifier (EG&G 7265) into 1f and 2f components to yield a retardation induced by the sample. Knowing the sample thickness, the retardation was recalculated into optical birefringence. Samples were prepared in 4.9-micron-thick cells with planar anchoring. The alignment quality was checked prior to measurement by inspection under the polarised light optical microscope.

2.4. Dielectric spectroscopy

The complex dielectric permittivity, ε^*, was studied using a Solatron 1260 impedance analyser. Measurements were conducted in the 1 Hz – 1 MHz frequency (f) range, with a probe voltage of 20 mV, and it was checked by optical observations that such a voltage is below the Fredericks transition threshold. The material was placed in 9.7-μm-thick glass cells with ITO electrodes and no polymer aligning layers. The lack of a surfactant layer resulted in the random configuration of the director in the LC phases; microscopic observations of optical textures suggested a dominant planar orientation without a preferable direction of the long molecular axis. The relaxation frequency, f_r, and dielectric strength of the mode, $\Delta\varepsilon$, were evaluated by fitting the complex dielectric permittivity to the Cole-Cole formula:

$$\varepsilon - \varepsilon_\infty = \frac{\Delta\varepsilon}{\sum\left(1+\frac{if}{f_r}\right)^{1-\alpha}} + i\left(\frac{\delta}{2\pi\varepsilon_0 f}\right),$$

where ε_∞ is the high frequency dielectric constant, α is the distribution parameter of the mode and δ is the low frequency conductivity, respectively.

2.5. Molecular modelling

The geometric parameters of the **1**-*n* series and **2**-*n* dimers were obtained using quantum mechanical DFT calculations with Gaussian09 software [56]. Optimisation of the molecular structures was carried out at the B3LYP/6-31 G(d) level of theory. Visualisations of electronic surfaces and ball-and-stick models were generated from the optimised geometries using the GaussView 5 software [57], and visualisations of the space-filling were produced post-optimisation using the QuteMol package [58].

3. Results and discussion

The transitional properties of the **1**-*n* series are listed in Table 1. All the members of the series exhibit an enantiotropic nematic phase except for **1**-3 which is a monotropic nematogen. The nematic phases were identified by the observation of a characteristic schlieren texture containing both two- and four-brush point singularities, see Figure 3, and which flashed when subjected to mechanical stress when viewed under the polarised light microscope. It is interesting to note that the nematic phases shown by these dimers exhibit extensive supercooling, and in some cases nematic behaviour at room temperature is observed prior to crystallisation.

The dependence of the transition temperatures on the number of methylene groups in the flexible spacer is shown for the **1**-*n* series in Figure 4. A distinct alternation is seen for both the melting points and the nematic-isotropic transition temperatures, T_{NI}, on increasing the length of the spacer in which the even-membered dimers exhibit the higher values. This alternation is

Table 1. The transitional properties of the **1**-*n* series.

n	$T_{Cr.}$/°C	$\Delta S_{Cr.}$/R	T_{NI}/°C	ΔS_{NI}/R
3†	178.6	14.3	120.1	0.04
4	180.0	12.7	230.9	0.93
5	140.2	15.1	156.7	0.13
6	166.7	16.9	206.9	0.88
7	139.2	13.3	159.7	0.27
8	153.2	19.1	186.8	0.94
9	136.5	13.9	155.7	0.32
10	164.4	20.5	168.7	0.85
11	128.2	17.7	150.1	0.38
12	134.8	18.1	160.4	0.86

†Data extracted on a cooling DSC cycle.

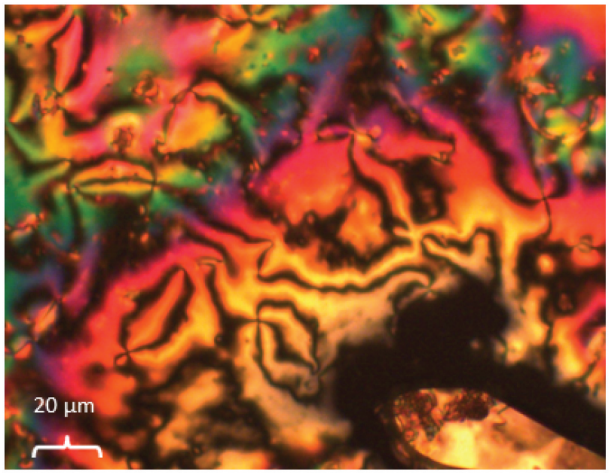

Figure 3. (Colour online) The nematic schlieren texture observed for **1**-6 (T=114°C).

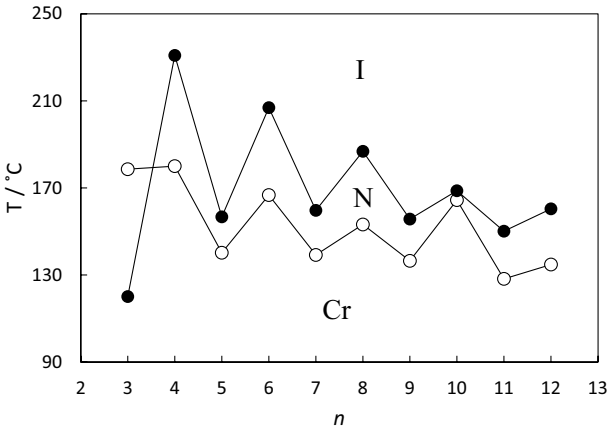

Figure 4. The dependence of the transition temperatures on the number of carbon atoms, n, in the spacer for the **1**-n series: open circles represent melting points and filled circles nematic-isotropic transitions.

more regular in the case of the dependence of T_{NI} and is most often attributed to the change in the average molecular shape on varying the parity of the spacer. Thus, for an even-membered spacer the mesogenic units are more or less parallel and the molecule is linear, see Figure 5, whereas for an odd-membered spacer the mesogenic groups are inclined at some angle with respect to each other and the molecule is bent, see Figure 6. The linear structure of an even membered dimer is then considered to be more compatible with the nematic environment than the bent shape of an odd-membered dimer, and this enhanced compatibility gives rise to the higher values of T_{NI}. Although intuitively pleasing, this explanation would predict that the entropy change associated with the nematic-isotropic transition, $\Delta S_{NI}/R$, shown by an even-membered dimer should be comparable with that of a conventional low molar mass mesogen based on a single mesogenic unit whereas that exhibited by a bent odd-membered dimer should be considerably smaller. Figure 7 shows the dependence of $\Delta S_{NI}/R$ on increasing the spacer length for the **1**-n series and a pronounced alternation is observed in which the even members show the higher values. Indeed, the values shown by the even members are several times larger than those seen for the adjacent odd members. It must be stressed that values of $\Delta S_{NI}/R$ shown by the odd members are more similar to those typically seen for conventional low molar mass mesogens [59] whereas those for the even members are much larger. To account for the dramatic alternation seen in the transitional properties of dimers on varying the parity of the spacer we must explicitly consider the flexibility of the spacer [49]. In the isotropic phase, approximately half the

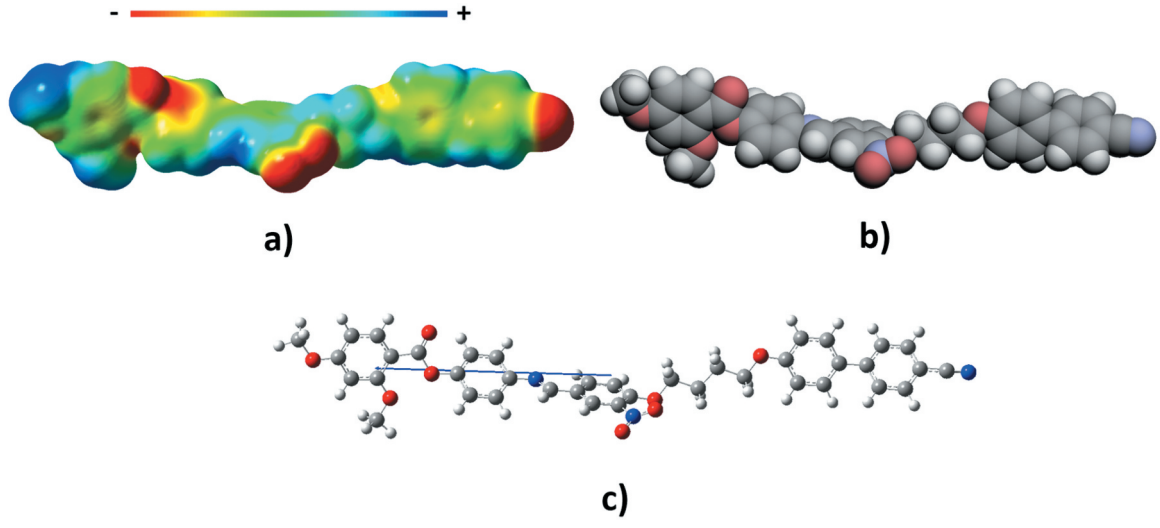

Figure 5. (Colour online) (a) The electrostatic potential surface in which red indicates electron rich and blue electron poor regions of the molecule, (b) space filling model and (c) ball and stick model indicating the dipole moment of **1**-4.

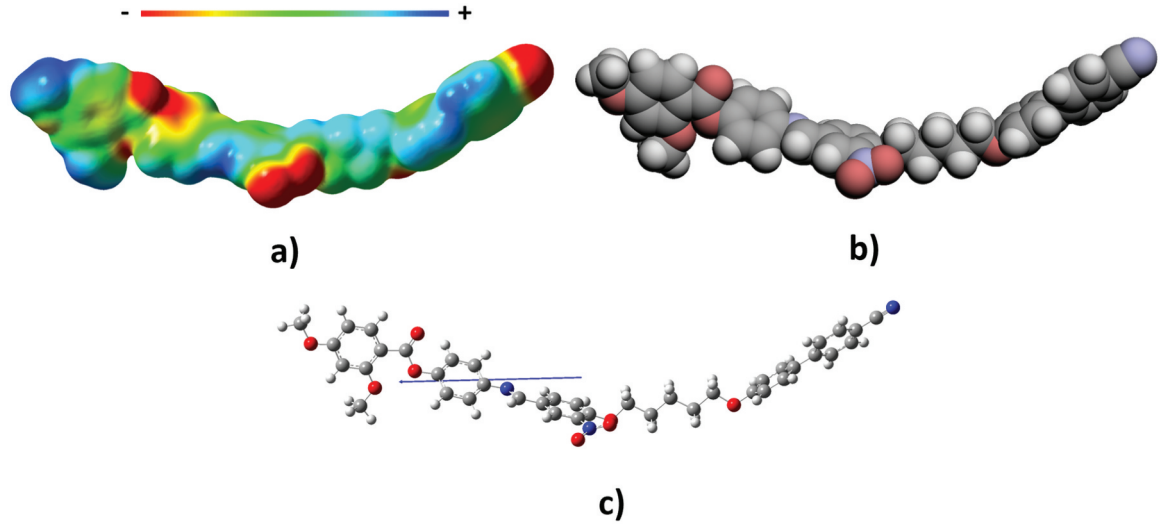

Figure 6. (Colour online) (a) The electrostatic potential surface in which red indicates electron rich and blue electron poor regions of the molecule, (b) space filling model and (c) ball and stick model showing the dipole moment of **1**-5.

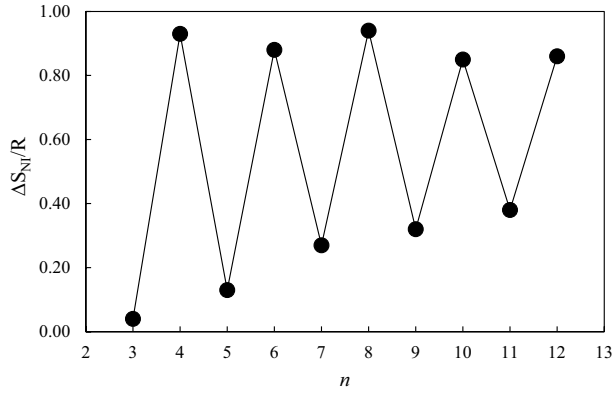

Figure 7. The dependence of the nematic-isotropic entropy change scaled by the gas constant, $\Delta S_{NI}/R$, on the number of carbon atoms, *n*, in the spacer for the **1**-*n* series.

conformations of an even-membered dimer are more or less linear whereas this falls to just 10% for an odd-membered dimer. At the transition to the nematic phase, the more elongated conformers are favoured and the extent to which the conformational distribution of the molecules can be changed depends on the conformational energy of the more anisotropic conformers which is higher for odd- than even-membered dimers. Thus, at the transition to the nematic phase many of the bent conformers are converted to linear conformers for an even-membered dimer and this enhances the orientational order of the N phase giving larger values of $\Delta S_{NI}/R$ than would be expected for a conventional low molar mass mesogen. By comparison for an odd-membered dimer the difference in energy between the bent and linear conformers is too large for the orientational order of the nematic phase to drive their interconversion. In consequence, the orientational order of the nematic phase is not increased in the same manner as for an even-membered dimer, and the values of $\Delta S_{NI}/R$ observed for an odd-membered dimer are smaller. This synergy between conformational and orientational order has been captured in molecular field theories that reveal the attenuation seen in the alternation of T_{NI}, see Figure 4, may be accounted for in terms of torsional fluctuations about the energy minima of conformations that result in reduced orientational correlations [60]. We note that the values of $\Delta S_{NI}/R$ listed in Table 1 for both odd and even members of the **1**-*n* series are lower than often observed for both symmetric [9,60,61] and non-symmetric liquid crystal dimers [10]. This may be attributed to the increase in molecular biaxiality associated with the methoxy and nitro lateral substituents attached to the benzylideneaniline benzoate moiety that reduces the orientational order of the nematic phase and hence, a smaller value of $\Delta S_{NI}/R$ is observed. Similarly, low values of $\Delta S_{NI}/R$ have been observed for dimers containing bulky pyrene- or cholesteryl-based mesogenic units [62,63].

The alternation seen in the melting points of the **1**-*n* series although less regular than that seen for T_{NI}, Figure 4, has been interpreted for other nematogenic dimer series as indicating that the change in the conformational statistical weights of the spacer on melting is small for even-membered spacers but large for odd-members. It may also reflect, however, the ease of packing of even-membered dimers into a crystal lattice given their more linear shapes compared to that of bent odd members.

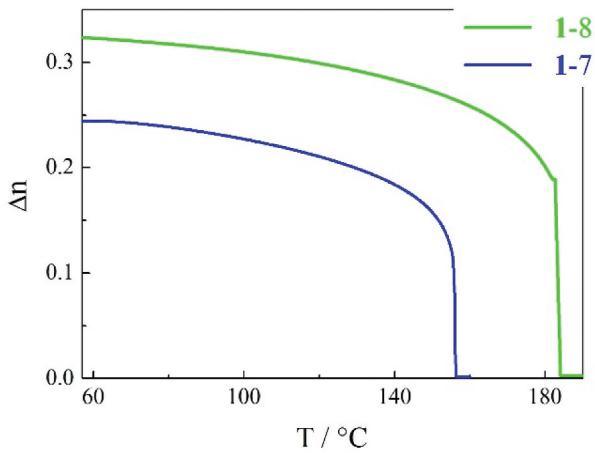

Figure 8. (Colour online) Temperature dependence of optical birefringence for compounds **1**-8 (green line) and **1**-7 (blue line).

The temperature dependence of the optical birefringence of an even-membered (**1**-8) and odd-membered (**1**-7) dimer is compared in Figure 8. It is clear that the bent shape of **1**-7 results in a reduction in molecular anisotropy and leads to a strong reduction in optical birefringence compared to that shown by the linear **1**-8; Δn_{max}, which represents the birefringence value extrapolated to the ideally ordered state (S = 1), is 0.40 and 0.32, for **1**-8 and **1**-7, respectively. The values were obtained from the fitting of the measured birefringence to a critical temperature dependence: $\Delta n = \Delta n_{max}(\frac{T_c - T}{T_c})^{\beta}$. This behaviour is in accord with that found for other liquid crystal dimers [64].

The dielectric spectroscopy studies performed for compound **1**-7 revealed a relatively high permittivity value, of the order of 200. A relaxation mode evolves smoothly through the transition from the isotropic to the nematic phase, see Figure 9, and thus it should be attributed to non-collective molecular fluctuations. The low relaxation frequency (below 100 Hz), and its decrease seen in the nematic phase on cooling, results from the increasing viscosity of the material composed of non-linear dimeric molecules. The high value of ε evidences the strong dipole moment of the molecules in accord with Meier-Maier theory [65,66] that predicts that the dielectric permittivity in the isotropic and nematic phases is proportional to the square of the molecular dipole moment. It should be noted that a permittivity of the same order of magnitude has been reported for other strongly polar nematogens [67]. The values measured here, however, are higher suggesting that local short-range ferroelectric order contributes to an increase of the dielectric mode strength. We note that normally in the nematic phase a local antiferroelectric arrangement of the dipoles is found (that may lead to a reversal in the sign of the dielectric anisotropy). In comparison, for the compounds studied here it would appear reasonable to expect ferroelectric correlations given that these molecules contain structural fragments similar to those known to promote the formation of the ferroelectric nematic phase.

The rationale underpinning the molecular design of the **1**-*n* series was to prepare dimers in which the dipole moments associated with the two mesogenic units lie more or less parallel to each other. The calculated dipole moment of benzylideneaniline benzoate fragment, described as [4-[(E)-(4-methoxy-3-nitrophenyl)methylideneamino]phenyl] 2,4-dimethoxybenzoate is 6.20 D and for 4-methoxycyanobiphenyl, representing the cyanobiphenyl moiety, is 6.49 D; these are shown in Figure ES1. The calculated dipole moment for **1**-4 is

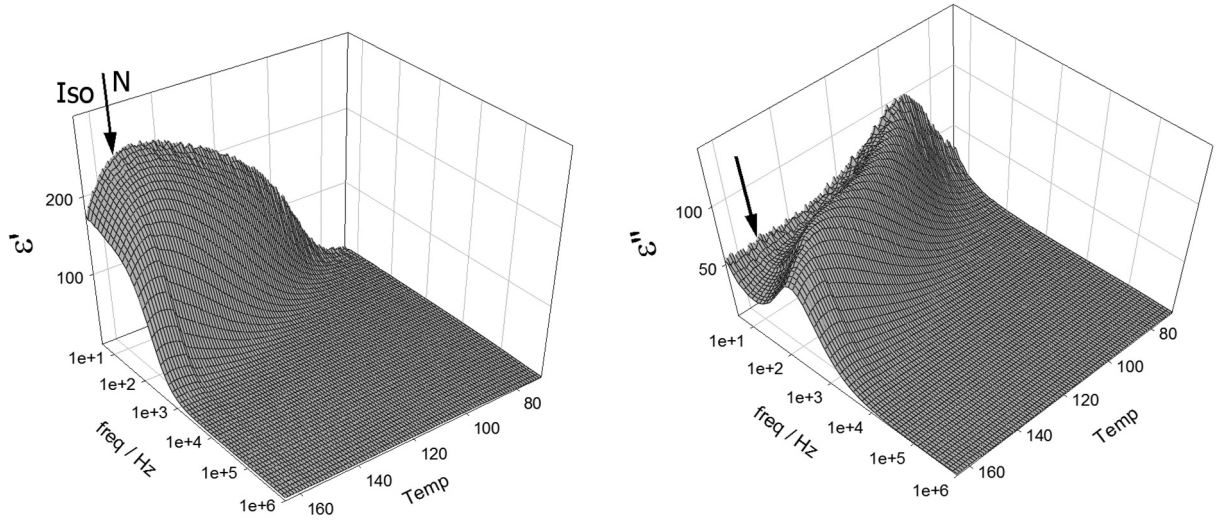

Figure 9. Real (ε ′) and imaginary (ε ″) parts of permittivity, measured as a function of temperature and frequency for compound **1**-7.

Table 2. The transitional properties of the **2**-*n* dimers.

n	T_{Cr-}/°C	ΔS_{Cr-}/R	T_{NI}/°C	ΔS_{NI}/R
5	180.6	14.7	69.0	–[†]
6	158.1	14.5	95.4	0.24

[†]Measured using POM.

12.75 D, and lies approximately along the molecular long axis, Figure 5. The dipole moment of **1**-4 is essentially the sum of those of the two mesogenic moieties as expected. The calculated molecular dipole moment of **1**-5 is 11.09 D and lower than that calculated for **1**-4. This reflects the bent shape of **1**-5 (Figure 6) such that the dipole moments of the two mesogenic units are now inclined with respect to each other.

The transitional properties of the **2**-*n* dimers are listed in Table 2, and both dimers show a monotropic nematic phase assigned on the basis of the observation of a characteristic schlieren texture as described earlier, Figure 10. The value of T_{NI} shown by **2**-6 is around 26 K higher than that shown by **2**-5, a much smaller difference than seen between **1**-6 and **1**-5 of 50 K. This may be accounted for in terms of the change in molecular shape arising from moving the spacer link from the *para* to the *meta* position, see Figures 11 and Figure 12. The reduction in the value of T_{NI} on moving from **1**-6 to **2**-6 is 111.5 K and between **1**-5 and **2**-5 is 87.7 K. These changes reflect that the change in the linking position of the spacer to the benzylideneaniline benzoate moiety reduces the structural anisotropy of both the odd and even members but that this is greater in the case of an

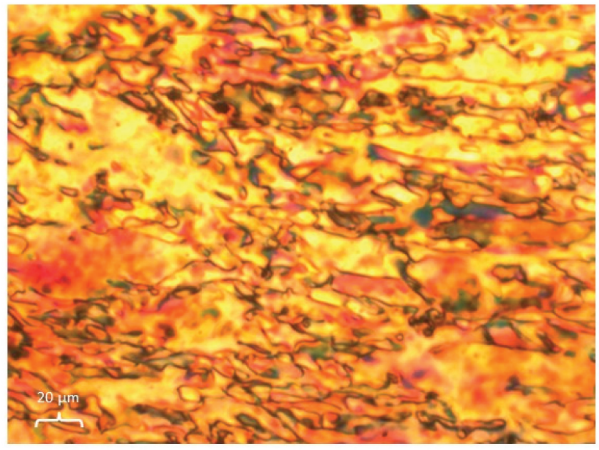

Figure 10. (Colour online) The nematic schlieren texture shown by **2**-6 (T = 90°C).

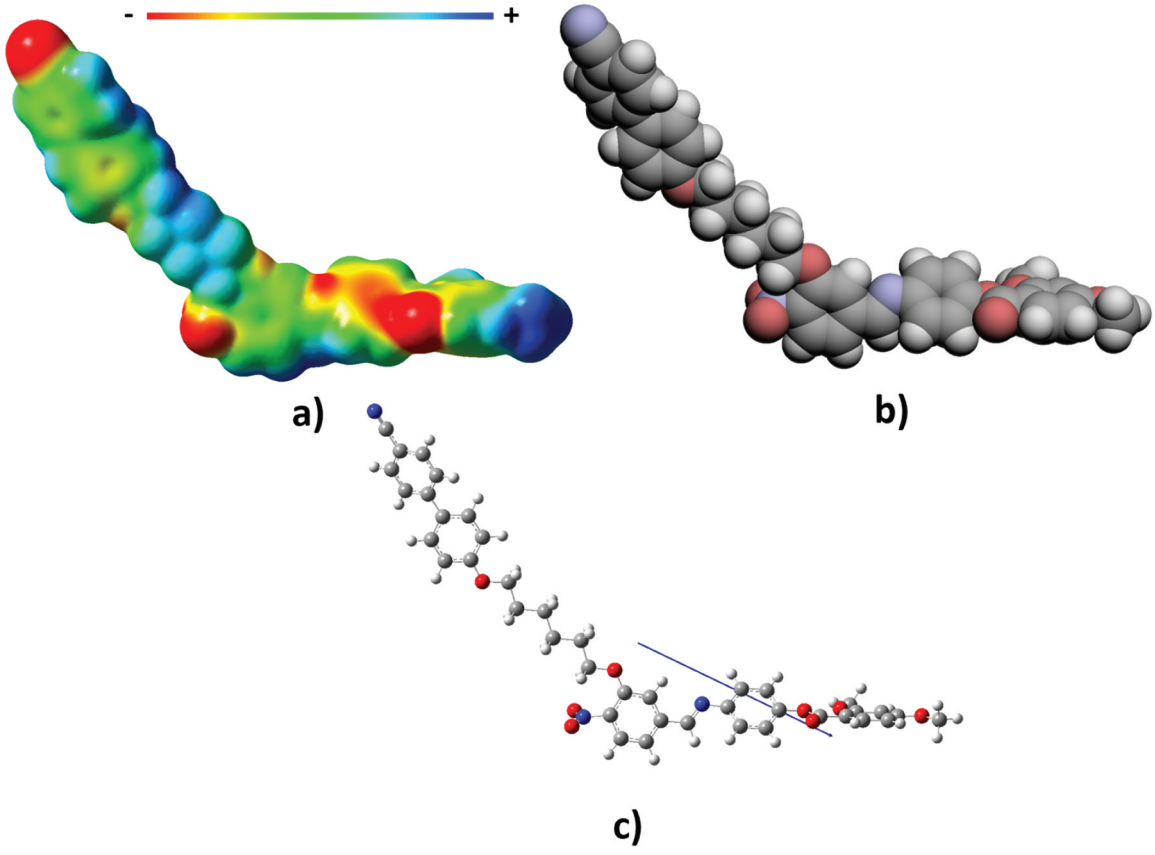

Figure 11. (Colour online) (a) The electrostatic potential surface in which red indicates electron rich and blue electron poor regions of the molecule, (b) space filling model, and (c) ball and stick model showing the dipole moment of **2**–6.

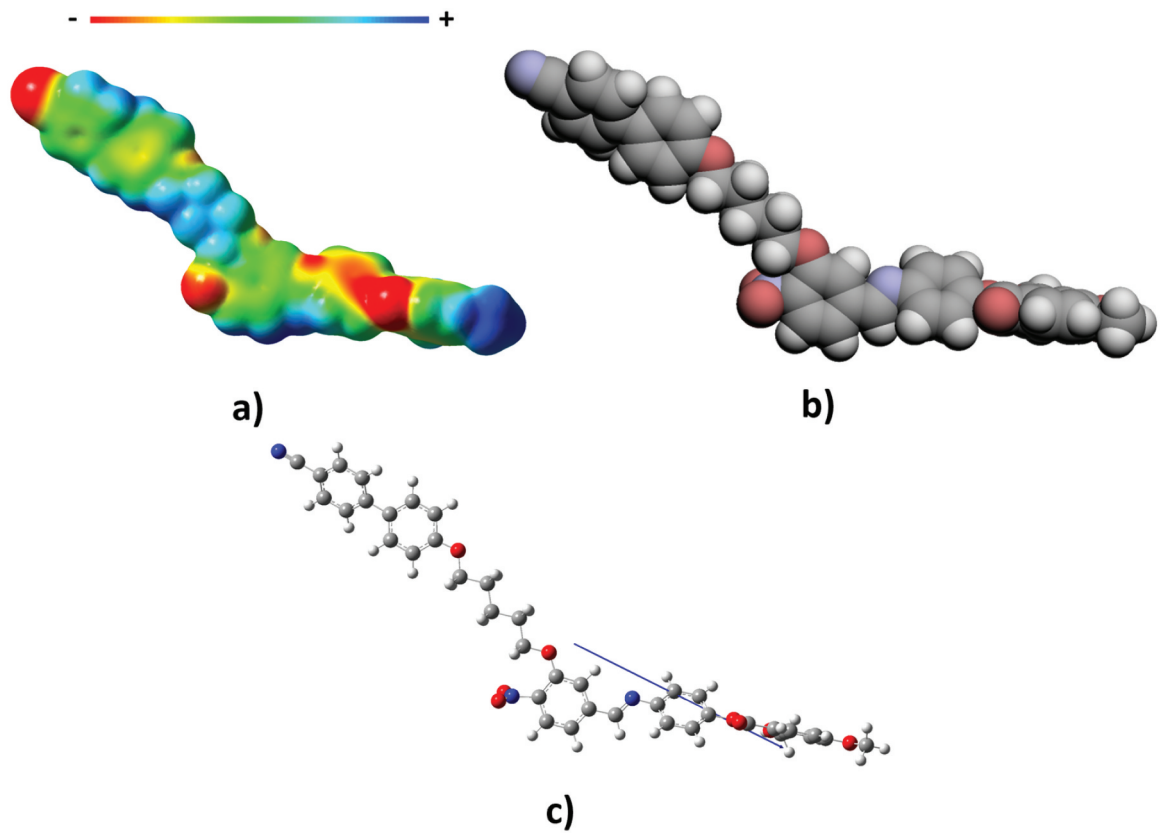

Figure 12. (Colour online) (a) The electrostatic potential surface in which red indicates electron rich and blue electron poor regions of the molecule, (b) space filling model and (c) ball and stick model showing the dipole moment of **2**–5.

even-membered spacer. Indeed, for a series of non-symmetric dimers containing terphenyl- and cholesteryl-based mesogenic units, this structural change inverted the sense of the alternation seen for the values of the clearing temperature and associated entropy changes [68]. This was attributed to the change in molecular shape such that there are more conformations that hold the mesogenic units more or less parallel for the odd-membered dimers than there are for the even-membered spacer. This inversion has not been observed here, but it is interesting to note that the melting point of **2**-5 is higher than that of **2**-6. This interpretation is also supported by the smaller value of $\Delta S_{NI}/R$ shown by **2**-6 of 0.24 compared to 0.88 for **1**-6. This reduction reflects the increased molecular biaxiality of the bent **2**-6 compared to that of the essentially linear **1**-6 that reduces the orientational order of the nematic phase and hence, a smaller value of $\Delta S_{NI}/R$ is observed [62].

The calculated molecular dipole moment for **2**-5, 12.60 D, is higher than that seen for **2**-6, 12.01 D. This again reflects the change in molecular shape arising from linking the spacer to the *meta* position on the benzylideneaniline benzoate moiety. The strongly monotropic nature of the materials precluded their characterisation using dielectric spectroscopy, although the schlieren texture observed (Figure 10) indicates the formation of a conventional nematic phase.

The dimers reported here have molecular dipole moments similar in magnitude to those commonly reported for conventional low molar mass ferroelectric nematogens [69]. Although dielectric studies possibly indicate local short-range ferroelectric order in the nematic phase (Figure 9), we find no evidence that these dimers exhibit the N_F phase. It has emerged that a key structural feature promoting the formation of the N_F phase in conventional mesogens is regions of alternating electron density [69]. This is consistent with a molecular model developed by Madhusudana in which the molecules are considered to possess longitudinal surface charge density waves and these interact inhibiting the formation of antiparallel structures [70]. In practice, this type of structure is most commonly achieved by using ester links within the mesogenic unit to inhibit electron delocalisation creating regions of alternating electron density. The design of our first-generation materials reported here focussed on the principle of parallel dipole moments and the

structures of the mesogenic units were not optimised in terms of achieving a given electron density profile. This is apparent in the electrostatic potential surfaces shown in Figures 5, 6, 11 and Figure 12. Furthermore, it is well known that the cyanobiphenyl fragment has a strong tendency to form antiparallel associations [71]. Our next focus now is to modify the structures of the mesogenic units in an attempt to promote the formation of the N_F phase.

4. Conclusions

We have reported the liquid crystal behaviour of a series of dimers, **1**-*n*, in which the dipole moments of the mesogenic units are parallel giving rise to a large molecular longitudinal dipole moment. The dimers are exclusively nematogenic and their transitional properties, T_{NI} and $\Delta S_{NI}/R$, alternate on varying the length and parity of the flexible spacer. This archetypal behaviour is attributed to changes in average molecular shape and molecular flexibility. The high value of the dielectric permittivity measured for **1**-7 reflects the strong dipole moment of the molecule and possibly indicates local short-range ferroelectric order. Changing the linking position of the spacer to the benzylideneaniline benzoate fragment from *para* to *meta* reduces the difference in shape between odd and even-membered dimers and this is reflected in the transition temperatures. Again, these dimers are exclusively nematogenic. In the dimer reported to exhibit a ferroelectric nematic phase, the mesogenic unit dipoles are antiparallel, and it was suggested that there was a strong tendency for these to adopt U-shaped conformations, stabilised by dipolar interactions, that drive the formation of the N_F phase [37]. By comparison, the properties of the dimers reported here are wholly consistent with the molecules adopting extended conformations rather than being dominated by U-shaped conformations that would presumably minimise dipolar energy. The physical significance of this differing behaviour is unclear, and we intend to study the effects of varying the structures of the mesogenic units in an attempt to promote ferroelectric ordering.

Disclosure statement

No potential conflict of interest was reported by the author(s).

Funding

C.T.I. and J.M.D.S. acknowledge the financial support of the Engineering and Physical Sciences Research Council [EP/V048775/1]. D.P. gratefully thanks the National Science Centre (Poland) under the grant no. [2021/43/B/ST5/00240].

ORCID

Ewan Cruickshank http://orcid.org/0000-0002-4670-8405
Damian Pociecha http://orcid.org/0000-0001-7734-3181
Ewa Gorecka http://orcid.org/0000-0002-8076-5489
Corrie T. Imrie http://orcid.org/0000-0001-6497-5243

References

[1] Tomczyk W, Longa L. Role of molecular bend angle and biaxiality in the stabilization of the twist-bend nematic phase. Soft Matter. 2020;16(18):4350–4357. doi: 10.1039/d0sm00078g
[2] Kubala P, Ciesla M, Longa L. Splay-induced order in systems of hard tapers. Phys Rev E. 2023;108(5):054701. doi: 10.1103/PhysRevE.108.054701
[3] Imrie CT, Henderson PA. Liquid crystal dimers and higher oligomers: between monomers and polymers. Chem Soc Rev. 2007;36:2096–2124. doi: 10.1039/b714102e
[4] Imrie CT, Henderson PA, Yeap GY. Liquid crystal oligomers: going beyond dimers. Liq Cryst. 2009;36(6–7):755–777. doi: 10.1080/02678290903157455
[5] Vorländer D. Über die Natur der Kohlenstoffketten in kristallin-flüssigen Substanzen. Z Phys Chem. 1927;126(1):449–472. doi: 10.1515/zpch-1927-12629
[6] Griffin AC, Britt TR. Effect of molecular-structure on mesomorphism.12. Flexible-center siamese-twin liquid-crystalline diesters – a prepolymer model. J Am Chem Soc. 1981;103(16):4957–4959. doi: 10.1021/ja00406a056
[7] Luckhurst GR. Liquid-crystal dimers and oligomers – experiment and theory. Macromolec Symp. 1995;96(1):1–26. doi: 10.1002/masy.19950960103
[8] Emsley JW, Luckhurst GR, Shilstone GN, et al. The preparation and properties of the α,ω-bis(4,4′-cyanobiphenyloxy)alkanes: nematogenic molecules with a flexible core. Mol Cryst Liq Cryst. 1984;102(8–9):223–233. doi: 10.1080/01406568408070532
[9] Date RW, Imrie CT, Luckhurst GR, et al. Smectogenic dimeric liquid crystals. The preparation and properties of the α,ω-bis(4- n -alkylanilinebenzylidine-4′-oxy) alkanes. Liq Cryst. 1992;12(2):203–238. doi: 10.1080/02678299208030393
[10] Hogan JL, Imrie CT, Luckhurst GR. Asymmetric dimeric liquid crystals the preparation and properties of the α-(4-cyanobiphenyl-4'-oxy)-ω-(4-n-alkylanil inebenzylidene-4'-oxy)hexanes. Liq Cryst. 1988;3(5):645–650. doi: 10.1080/02678298808086408
[11] Attard GS, Date RW, Imrie CT, et al. Non-symmetric dimeric liquid crystals the preparation and properties of the α-(4-cyanobiphenyl-4′-yloxy)-ω-(4-n-alkylanilineben zylidene-4′-oxy)alkanes. Liq Cryst. 1994;16(4):529–581. doi: 10.1080/02678299408036531
[12] Imrie CT. Non-symmetric liquid crystal dimers: how to make molecules intercalate. Liq Cryst. 2006;33(11–12):1449–1454. doi: 10.1080/02678290601140498

[13] Walker R, Pociecha D, Storey JMD, et al. Remarkable smectic phase behaviour in odd-membered liquid crystal dimers: the CT6O. m series. J Mater Chem C. 2021;9(15):5167–5173. doi: 10.1039/D1TC00904D
[14] Walker R, Pociecha D, Faidutti C, et al. Remarkable stabilisation of the intercalated smectic phases of non-symmetric dimers by tert-butyl groups. Liq Cryst. 2022;49:969–981. doi: 10.1080/02678292.2022.2055797
[15] Cestari M, Diez-Berart S, Dunmur DA, et al. Phase behavior and properties of the liquid-crystal dimer 1″,7″-bis(4-cyanobiphenyl-4′-yl) heptane: a twist-bend nematic liquid crystal. Phys Re E. 2011;84(3):031704. doi: 10.1103/PhysRevE.84.031704
[16] Borshch V, Kim YK, Xiang J, et al. Nematic twist-bend phase with nanoscale modulation of molecular orientation. Nature Commun. 2013;4(1):2635. doi: 10.1038/ncomms3635
[17] Chen D, Porada JH, Hooper JB, et al. Chiral heliconical ground state of nanoscale pitch in a nematic liquid crystal of achiral molecular dimers. Proc Natl Acad Sci USA. 2013;110:15931–15936. doi: 10.1073/pnas.1314654110
[18] Henderson PA, Imrie CT. Methylene-linked liquid crystal dimers and the twist-bend nematic phase. Liq Cryst. 2011;38(11–12):1407–1414. doi: 10.1080/02678292.2011.624368
[19] Paterson DA, Abberley JP, Harrison WT, et al. Cyanobiphenyl-based liquid crystal dimers and the twist-bend nematic phase. Liq Cryst. 2017;44:127–146. doi: 10.1080/02678292.2016.1274293
[20] Cruickshank E, Salamonczyk M, Pociecha D, et al. Sulfur-linked cyanobiphenyl-based liquid crystal dimers and the twist-bend nematic phase. Liq Cryst. 2019;46(10):1595–1609. doi: 10.1080/02678292.2019.1641638
[21] Mandle RJ. A ten-year perspective on twist-bend nematic materials. Molecules. 2022;27(9):2689. doi: 10.3390/molecules27092689
[22] Paterson DA, Walker R, Abberley JP, et al. Azobenzene-based liquid crystal dimers and the twist-bend nematic phase. Liq Cryst. 2017;44:2060–2078. doi: 10.1080/02678292.2017.1366075
[23] Walker R, Pociecha D, Storey JMD, et al. The chiral twist-bend nematic phase (N^*_{TB}). Chem Eur J. 2019;25(58):13329–13335. doi: 10.1002/chem.201903014
[24] Abberley JP, Killah R, Walker R, et al. Heliconical smectic phases formed by achiral molecules. Nat Commun. 2018;9:228. doi: 10.1038/s41467-017-02626-6
[25] Salamonczyk M, Vaupotic N, Pociecha D, et al. Multi-level chirality in liquid crystals formed by achiral molecules. Nature Commun. 2019;10(1):1922. doi: 10.1038/s41467-019-09862-y
[26] Pociecha D, Vaupotic N, Majewska M, et al. Photonic bandgap in achiral liquid crystals—a twist on a twist. Adv Mat. 2021;33(39):2103288. doi: 10.1002/adma.202103288
[27] Alshammari AF, Pociecha D, Walker R, et al. New patterns of twist-bend liquid crystal phase behaviour: the synthesis and characterisation of the 1-(4-cyanobiphenyl-4′-yl)-10-(4-alkylaniline-benzylidene-4′-oxy) decanes (CB10O· m). Soft Matter. 2022;18(25):4679–4688. doi: 10.1039/D2SM00162D
[28] Imrie CT, Walker R, Storey JMD, et al. Liquid crystal dimers and smectic phases from the intercalated to the twist-bend. Crystals. 2022;12(9):1245. doi: 10.3390/cryst12091245
[29] Cruickshank E, Walker R, Strachan GJ, et al. The influence of the imine bond direction on the phase behaviour of symmetric and non-symmetric liquid crystal dimers. J Molec Liq. 2023;391:123226. doi: 10.1016/j.molliq.2023.123226
[30] Cruickshank E, Anderson K, Storey JMD, et al. Helical phases assembled from achiral molecules: twist-bend nematic and helical filamentary B4 phases formed by mesogenic dimers. J Molec Liq. 2022;346:118180. doi: 10.1016/j.molliq.2021.118180
[31] Imrie CT, Luckhurst GR. Liquid crystal trimers: the synthesis and characterisation of the 4,4′-bis ω-(4-cyanobiphenyl-4′-yloxy)alkoxy biphenyls. J Mater Chem. 1998;8:1339–1343. doi: 10.1039/a801128a
[32] Imrie CT, Henderson PA, Seddon JM. Non-symmetric liquid crystal trimers. The first example of a triply-intercalated alternating smectic C phase. J Mater Chem. 2004;14(16):2486–2488. doi: 10.1039/b404319g
[33] Tuchband MR, Paterson DA, Salamonczykc M, et al. Distinct differences in the nanoscale behaviors of the twist–bend liquid crystal phase of a flexible linear trimer and homologous dimer. Proc Natl Acad Sci USA. 2019;116(22):10698–10704. doi: 10.1073/pnas.1821372116
[34] Henderson PA, Imrie CT. Liquid crystal tetramers: influence of molecular shape on liquid crystal behaviour. Liq Cryst. 2005;32(11–12):1531–1541. doi: 10.1080/02678290500410620
[35] Majewska MM, Forsyth E, Pociecha D, et al. Controlling spontaneous chirality in achiral materials: liquid crystal oligomers and the heliconical twist-bend nematic phase. Chem Commun. 2022;58(34):5285–5288. doi: 10.1039/D1CC07012F
[36] Imrie CT, Stewart D, Rémy C, et al. Liquid crystal tetramers. J Mater Chem. 1999;9(10):2321–2325. doi: 10.1039/a901899i
[37] Nakasugi S, Kang S, Chang TFM, et al. Three distinct polar phases, isotropic, nematic, and Smectic-A phases, formed from a fluoro-substituted dimeric molecule with large dipole moment. J Phys Chem B. 2023;127(29):6585–6595. doi: 10.1021/acs.jpcb.3c02259
[38] Nishikawa H, Shiroshita K, Higuchi H, et al. A fluid liquid-crystal material with highly polar order. Adv Mater. 2017;29(43):1702354. doi: 10.1002/adma.201702354
[39] Mandle RJ, Cowling SJ, Goodby JW. A nematic to nematic transformation exhibited by a rod-like liquid crystal. Phys Chem Chem Phys. 2017;19(18):11429–11435. doi: 10.1039/C7CP00456G
[40] Chen X, Korblova E, Dong DP, et al. First -principles experimental demonstration of ferroelectricity in a thermotropic nematic liquid crystal: polar domains and striking electro-optics. Proc Natl Acad Sci USA. 2020;117(25):14021–14031. doi: 10.1073/pnas.2002290117
[41] Manabe A, Bremer M, Kraska M. Ferroelectric nematic phase at and below room temperature. Liq Cryst. 2021;48:1079–1086. doi: 10.1080/02678292.2021.1921867

[42] Mandle RJ, Cowling SJ, Goodby JW. Structural variants of RM734 in the design of splay nematic materials. Liq Cryst. 2021;48(12):1780–1790. doi: 10.1080/02678292.2021.1934740
[43] Mandle RJ. A new order of liquids: polar order in nematic liquid crystals. Soft Matter. 2022;18(27):5014–5020. doi: 10.1039/D2SM00543C
[44] Song YH, Li JX, Xia RL, et al. Development of emergent ferroelectric nematic liquid crystals with highly fluorinated and rigid mesogens. Phys Chem Chem Phys. 2022;24(19):11536–11543. doi: 10.1039/D2CP01110G
[45] Li JX, Wang ZD, Deng MH, et al. General phase-structure relationship in polar rod-shaped liquid crystals: Importance of shape anisotropy and dipolar strength. Giant. 2022;11:100109. doi: 10.1016/j.giant.2022.100109
[46] Brown S, Cruickshank E, Storey JMD, et al. Multiple polar and non-polar nematic phases. Chemphyschem. 2021;22(24):2506–2510. doi: 10.1002/cphc.202100644
[47] Cruickshank E, Walker R, Storey JMD, et al. The effect of a lateral alkyloxy chain on the ferroelectric nematic phase. RSC Adv. 2022;12(45):29482–29490. doi: 10.1039/D2RA05628C
[48] Tufaha N, Cruickshank E, Pociecha D, et al. Molecular shape, electronic factors, and the ferroelectric nematic phase: investigating the impact of structural modifications. Chem Eur J. 2023;29(28):e202300073. doi: 10.1002/chem.202300073
[49] Stepanafas G, Cruickshank E, Brown S, et al. Ferroelectric nematogens containing a methylthio group. Mater Adv. 2024;5(2):525–538. doi: 10.1039/D3MA00446E
[50] Cruickshank E, Tufaha N, Walker R, et al. The influence of molecular shape and electronic properties on the formation of the ferroelectric nematic phase. Liquid Crystals. 2024;(3):401–415. doi: 10.1080/02678292.2024.2304598
[51] Pociecha D, Walker R, Cruickshank E, et al. Intrinsically chiral ferronematic liquid crystals: an inversion of the helical twist sense at the chiral nematic - chiral ferronematic phase transition. J Molec Liq. 2022;361:119532. doi: 10.1016/j.molliq.2022.119532
[52] Cruickshank E, Rybak P, Majewska MM, et al. To be or not to be polar: the ferroelectric and antiferroelectric nematic phases. ACS Omega. 2023;8(39):36562–36568. doi: 10.1021/acsomega.3c05884
[53] Dai SQ, Li JX, Kougo JC, et al. Polar liquid crystalline polymers bearing mesogenic side chains with large dipole moment. Macromolecules. 2021;54(13):6045–6051. doi: 10.1021/acs.macromol.1c00864
[54] Li JX, Xia RL, Xu H, et al. How far can we push the rigid oligomers/polymers toward ferroelectric nematic liquid crystals? J Am Chem Soc. 2021;143:17857–17861. doi: 10.1021/jacs.1c09594
[55] Cruickshank E, Pearson A, Brown S, et al. The ferroelectric nematic phase: on the role of lateral alkyloxy chains. Liq Cryst. 2023;50(11–12):1960–1967. doi: 10.1080/02678292.2023.2221651
[56] Frisch MJ, Trucks GW, Schlegel HB, et al. Gaussian 09 (Revision D.01). Wallingford (CT): Gaussian Inc.; 2016.
[57] Dennington R, Keith T, Millam J. Gauss view, version 5. Shawnee Mission (KS): Semichem Inc.; 2009.
[58] Tarini M, Cignoni P, Montani C. Ambient occlusion and edge cueing to enhance real time molecular visualization. IEEE Trans Vis Comp Graphics. 2006;12(5):1237–1244. doi: 10.1109/TVCG.2006.115
[59] Henderson PA, Cook AG, Imrie CT. Oligomeric liquid crystals: from monomers to trimers. Liq Cryst. 2004;31(11):1427–1434. doi: 10.1080/02678290412331298067
[60] Luckhurst GR. Liquid crystals: a chemical physicist's view. Liq Cryst. 2005;32(11–12):1335–1364. doi: 10.1080/02678290500423128
[61] Arakawa Y, Komatsu K, Shiba T, et al. Phase behaviors of classic liquid crystal dimers and trimers: alternate induction of smectic and twist-bend nematic phases depending on spacer parity for liquid crystal trimers. J Mol Liq. 2021;326:115319. doi: 10.1016/j.molliq.2021.115319
[62] Attard GS, Imrie CT, Karasz FE. Low molar mass liquid-crystalline glasses –preparation and properties of the alpha-(4-cyanobiphenyl-4'-oxy)-omega-(1-pyreniminebenzylidene-4'-oxy)alk anes. Chem Mater. 1992;4(6):1246–1253. doi: 10.1021/cm00024a025
[63] Donaldson T, Staesche H, Lu ZB, et al. Symmetric and non-symmetric chiral liquid crystal dimers. Liq Cryst. 2010;37(8):1097–1110. doi: 10.1080/02678292.2010.494412
[64] Arakawa Y, Sasaki S, Igawa K, et al. Birefringence and photoluminescence properties of diphenylacetylene-based liquid crystal dimers. New J Chem. 2020;44(40):17531–17541. doi: 10.1039/D0NJ04426A
[65] Maier W, Meier G. Eine einfache Theorie der dielektrischen Eigenschaften homogen orientierter kristallinflüssiger Phasen des nematischen Typs. Z Naturforsch A. 1961;16(3):262–267. doi: 10.1515/zna-1961-0309
[66] Maier W, Meier G. Die Hauptdielektrizitätskonstanten der homogen geordneten kristallinflüssigen Phase des p-Azoxyanisols. Z Naturforsch A. 1961;16(5):470–477. doi: 10.1515/zna-1961-0504
[67] Czub J, Dabrowski R, Urban S, et al. Dielectric properties of strongly polar nematogens. Z Naturforsch A. 2010;65(3):221–230. doi: 10.1515/zna-2010-0311
[68] Marcelis ATM, Koudijs A, Sudhölter EJR. Dimer liquid crystals with bent mesogenic units. Liq Cryst. 2000;27(11):1515–1523. doi: 10.1080/026782900750018681
[69] Cruickshank E. The emergence of a polar nematic phase: a chemist's insight into the ferroelectric nematic phase. ChemPlusChem. 2024;e202300726. doi: 10.1002/cplu.202300726
[70] Madhusudana NV. Simple molecular model for ferroelectric nematic liquid crystals exhibited by small rod-like mesogens. Phys Rev E. 2021;104(1):014704. doi: 10.1103/PhysRevE.104.014704
[71] Dunmur DA. The magic of cyanobiphenyls: celebrity molecules. Liq Cryst. 2015;42:678–687. doi: 10.1080/02678292.2014.992056

Electronic Supplementary Information

A design approach to obtaining highly polar liquid crystal dimers

Amerigo Zattarin[a], Ewan Cruickshank[a,c], Damian Pociecha[b], John MD Storey[a], Ewa Gorecka[b], and Corrie T Imrie[a]*

[a]Department of Chemistry, School of Natural and Computing Sciences, University of Aberdeen, AB24 3UE, Scotland, United Kingdom; [b]Faculty of Chemistry, University of Warsaw, ul. Zwirki i Wigury 101, 02-089, Warsaw, Poland.

*Author for correspondence: email: c.t.imrie@abdn.ac.uk

[c]Present address: School of Pharmacy and Life Sciences, Robert Gordon University, Aberdeen, AB10 7GJ, United Kingdom.

1. General Information

1.1 Reagents

All reagents and solvents available commercially were purchased from Sigma Aldrich, Alfa Aesar, ACROS Organics, TCI Chemicals or Fluorochem and were used as received without further purification unless otherwise stated. If required, solvents were dried over molecular sieves for a minimum of 24 hours prior to use.

1.2 Thin Layer Chromatography

Reactions were monitored using thin layer chromatography, and the appropriate solvent system, using aluminium-backed plates with a coating of Merck Kieselgel 60 F254 silica purchased from Merck KGaA. The spots on the plates were visualised by UV light (254 nm) or by oxidation using an iodine dip.

1.3 Column Chromatography

For normal phase column chromatography, the separations were carried out using silica gel grade 60 Å, 40-63 µm particle size, purchased from Fluorochem and using an appropriate solvent system.

1.4 Structure Characterisation

All final products and intermediates that were synthesised were characterised using ^{1}H NMR, ^{13}C NMR and infrared spectroscopies. The ^{1}H and ^{13}C NMR spectra were recorded on either a 400 MHz Bruker Avance III HD NMR spectrometer, or a 300 MHz Bruker Ultrashield NMR spectrometer. The infrared spectra were recorded on a Thermal Scientific Nicolet IR100 FTIR spectrometer with an ATR diamond cell or a Perkin Elmer Spectrum 2 FTIR with an ATR diamond cell.

1.5 Purity Analysis

In order to determine the purity of the final products, elemental analysis was used. C, H, N microanalysis were carried out by the Sheffield Analytical and Scientific Services Elemental Microanalysis Service at the University of Sheffield using an Elementar Vario MICRO Cube. The instrument was calibrated using series of different masses of sulphanilamide and acetanilide. High-

resolution mass spectrometry was carried out at the University of Aberdeen by Dr Morag Douglas using a Waters XEVO G2 Q-Tof mass spectrometer. The instrument was calibrated with sodium formate, and the lock mass was leucine enkephalin, Formula: $C_{28}H_{37}N_5O_7$, $[M+H]^+$: 556.2771.

2. Synthesis and Analytical Data

2.1 [4[(E)-[4-[4-[ω-(4-cyanophenyl)phenoxy]alkyloxy]-3-nitrophenyl]methylideneamino]phenyl] 2,4-dimethoxybenzoates, 1-n series

The synthetic route used to obtain the **1**-*n* series is shown in Scheme ES1.

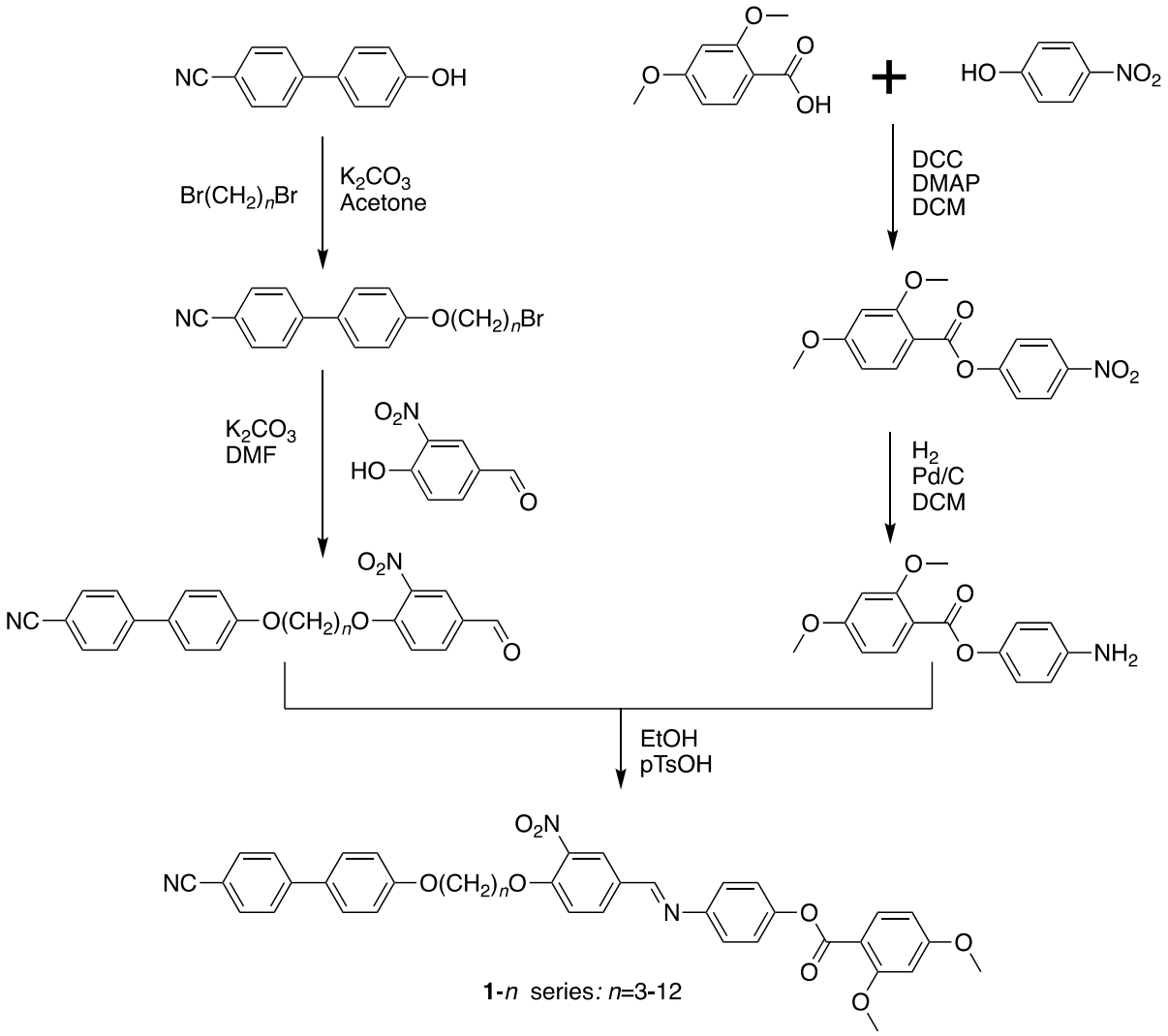

Scheme 1 The preparation of the **1**-*n* series.

2.1.1 4-{4-[(ω-Bromoalkyl)oxy]phenyl}benzonitriles

The 4-{4-[(ω-bromoalkyl)oxy]phenyl}benzonitriles were prepared as decribed in detail elsewhere [1]. 4-Cyano-4'-hydroxybiphenyl (6.6 mmol), the appropriate 1,ω-dibromoalkane (33 mmol eq.) and anhydrous potassium carbonate (26.4 mmol) were added to acetone (40 mL), and the reaction mixture refluxed with stirring for 24 h. The mixture was filtered, and the inorganic residue washed with copious amounts of acetone. The filtrate was concentrated in vacuo and allowed to stand for 3h at -20 °C. The resulting precipitate was collected and washed with hexane. The crude product was recrystallised from ethanol to give the title compound as a white solid. Yields in the range of 80-85 % were obtained.

4-{4-[(3-Bromopropyl)oxy]phenyl}benzonitrile

MP = 105 °C

^{1}H NMR (400 MHz, $CDCl_3$) δ 7.66 (q, J = 8.6 Hz, 4H), 7.54 (d, J = 8.7 Hz, 2H), 7.01 (d, J = 8.8 Hz, 2H), 4.17 (t, J = 5.8 Hz, 2H), 3.63 (t, J = 6.4 Hz, 2H), 2.35 (p, J = 6.1 Hz, 2H).

^{13}C NMR (101 MHz, $CDCl_3$) δ 159.34, 145.17, 132.61, 131.78, 128.43, 127.15, 119.10, 115.14, 110.19, 65.46, 32.28, 29.93.

IR $\bar{\nu}$ cm^{-1}: 2935,2869(aromatic CH), 2222(C≡N), 1602 (para di-substituted benzene).

4-{4-[(4-Bromobutyl)oxy]phenyl}benzonitrile

MP = 67 °C T_{NI} = 61 °C

^{1}H NMR (400 MHz, $CDCl_3$) δ 7.66 (d, *J* = 8.2 Hz, 4H), 7.53 (d, *J* = 8.9 Hz, 2H), 7.00 (d, *J* = 8.7 Hz, 2H), 4.06 (t, *J* = 6.0 Hz, 2H), 3.51 (t, *J* = 6.5 Hz, 2H), 2.19 – 1.93 (m, 4H).

^{13}C NMR (101 MHz, $CDCl_3$) δ 159.52, 145.21, 132.60, 131.58, 128.40, 127.12, 119.11, 115.07, 110.15, 67.03, 33.40, 29.45, 27.87.

IR $\bar{\nu}$ cm^{-1}: 293547,2871(aromatic CH), 2222(C≡N), 1601 (para di-substituted benzene).

4-{4-[(5-Bromopentyl)oxy]phenyl}benzonitrile

MP = 82 °C T_{NI} = 66 °C

^{1}H NMR (400 MHz, $CDCl_3$) δ 7.66 (q, *J* = 8.6 Hz, 4H, Ar), 7.53 (d, *J* = 8.7 Hz, 2H, Ar), 7.00 (d, *J* = 8.6 Hz, 2H, Ar), 4.02 (t, *J* = 6.3 Hz, 2H, ArO$\underline{CH_2}$$CH_2CH_2CH_2CH_2Br$)), 3.45 (t, *J* = 6.7 Hz, 2H, $ArOCH_2CH_2CH_2CH_2\underline{CH_2}Br$), 2.01 – 1.91 (m, 2H, $ArOCH_2\underline{CH_2}CH_2CH_2CH_2Br$), 1.91 – 1.80 (m, 2H, $ArOCH_2CH_2CH_2\underline{CH_2}CH_2Br$), 1.77 – 1.58 (m, 2H, $ArOCH_2CH_2\underline{CH_2}CH_2CH_2Br$).

^{13}C NMR (101 MHz, $CDCl_3$) δ 159.65, 145.24, 132.59, 131.44, 128.38, 127.11, 119.13, 115.10, 110.10, 67.76, 33.61, 32.47, 28.42, 24.85.

IR $\bar{\nu}$ cm^{-1}: 2945,2869(aromatic CH), 2224(C≡N), 1603 (para di-substituted benzene).

4-{4-[(6-Bromohexyl)oxy]phenyl}benzonitrile

MP = 60 °C T_{NI} = 69 °C

^{1}H NMR (400 MHz, $CDCl_3$) δ 7.66 (q, *J* = 8.2 Hz, 4H, Ar), 7.53 (d, *J* = 8.7 Hz, 2H, Ar), 6.99 (d, *J* = 8.6 Hz, 2H, Ar),4.02 (t, J = 6.4 Hz, 2H, ArO$\underline{CH_2}$(CH_2)$_5$Br), 3.43 (t, *J* = 6.7 Hz, 2H, ArO(CH_2)$_5$Br), 1.97 – 1.78 (m, 4H, ArO$CH_2\underline{CH_2}CH_2)_2\underline{CH_2}CH_2$Br), 1.62 – 1.44 (m, 4H, ArO$(CH_2)_2\underline{CH_2CH_2}(CH_2)_2$Br).

^{13}C NMR (101 MHz, $CDCl_3$) δ 159.73, 145.26, 132.59, 131.36, 128.36, 127.09, 119.14, 115.10, 110.08, 67.91, 33.83, 32.68, 29.07, 27.93, 25.31.

IR $\bar{\nu}$ cm^{-1}: 2921,2854(aromatic CH), 2225 (C≡N), 1600 (para di-substituted benzene).

4-{4-[(7-Bromoheptyl)oxy]phenyl}benzonitrile

MP = 66.3 °C T_{NI} = 68 °C

^{1}H NMR (400 MHz, $CDCl_3$) δ 7.66 (q, *J* = 8.5 Hz, 4H, Ar), 7.52 (d, *J* = 8.7 Hz, 2H, Ar), 6.99 (d, *J* = 8.9 Hz, 2H, Ar), 4.01 (t, *J* = 6.5 Hz, 2H, ArO$\underline{CH_2}$(CH_2)$_5$$CH_2$Br), 3.42 (t, J = 6.8 Hz, 2H, ArOCH_2(CH_2)$_5\underline{CH_2}$Br), 1.94 – 1.76 (m, 4H, ArO$CH_2\underline{CH_2}$(CH_2)$_3\underline{CH_2}CH_2$Br), 1.58 – 1.34 (m, 6H, ArO$CH_2CH_2(\underline{CH_2})_3CH_2CH_2$Br).

^{13}C NMR (101 MHz, $CDCl_3$) δ 159.77, 145.28, 132.58, 131.32, 128.35, 127.09, 119.14, 115.10, 110.07, 68.03, 33.95, 32.72, 29.13, 28.53, 28.09, 25.91.

IR $\bar{\nu}$ cm^{-1}: 2937,2854(aromatic CH), 2222 (C≡N), 1602 (para di-substituted benzene).

4-{4-[(8-Bromooctyl)oxy]phenyl}benzonitrile

MP = 80 °C T_{NI} = 69 °C

^{1}H NMR (400 MHz, $CDCl_3$) δ 7.68 (q, *J* = 8.6 Hz, 4H), 7.55 (d, *J* = 8.8 Hz, 2H), 7.02 (d, *J* = 8.6 Hz, 2H), 4.03 (t, *J* = 6.5 Hz, 2H, ArO$\underline{CH_2}CH_2CH_2CH_2$_$CH_2CH_2CH_2CH_2$Br), 3.44 (t, *J* = 6.8 Hz, 2H ArO$CH_2CH_2CH_2CH_2$__$CH_2CH_2CH_2\underline{CH_2}$Br), 1.95 – 1.78 (m, 6H, ArO$CH_2\underline{CH_2CH_2CH_2}$ $CH_2CH_2CH_2CH_2$Br), 1.57 – 1.33 (m, 6H, ArO$CH_2CH_2CH_2CH_2$ $\underline{CH_2CH_2CH_2}CH_2$Br).

^{13}C NMR (101 MHz, $CDCl_3$) δ 159.79, 145.28, 132.58, 131.29, 128.35, 127.09, 119.14, 115.10, 110.06, 68.10, 34.02, 32.79, 29.19, 28.70, 28.10, 25.96.

IR $\bar{\nu}$ cm^{-1}: 2920,2852(aromatic CH), 2235 (C≡N), 1604 (para di-substituted benzene).

4-{4-[(9-Bromononyl)oxy]phenyl}benzonitrile

MP = 71 °C T_{NI} = 70 °C

^{1}H NMR (400 MHz, $CDCl_3$) δ 7.68 (q, *J* = 8.7 Hz, 4H, Ar), 7.55 (d, *J* = 8.8 Hz, 2H, Ar), 7.01 (d, *J* = 9.0 Hz, 2H, Ar), 4.03 (t, *J* = 6.5 Hz, 2H, ArO$\underline{CH_2}(CH_2)_7CH_2Br$), 3.43 (t, *J* = 6.9 Hz, 2H, ArO$CH_2(CH_2)_7\underline{CH_2}Br$), 1.94 – 1.78 (m, 4H ArO$CH_2\underline{CH_2}CH_2CH_2CH_2CH_2CH_2\underline{CH_2}CH_2Br$), 1.56 – 1.31 (m, 10H ArO$CH_2CH_2\underline{CH_2CH_2CH_2CH_2CH_2}CH_2CH_2Br$).

^{13}C NMR (101 MHz, $CDCl_3$) δ 159.82, 145.28, 132.58, 131.26, 128.34, 127.08, 119.14, 115.11, 110.05, 68.15 34.06, 32.82, 29.36, 29.27, 29.22, 28.71, 28.16, 26.02.

IR $\bar{\nu}$ cm^{-1}: 2920,2852(aromatic CH), 2223 (C≡N), 1602 (para di-substituted benzene).

4-{4-[(10-Bromodecyl)oxy]phenyl}benzonitrile

MP = 72 °C T_{NI} = 68°C

^{1}H NMR (400 MHz, $CDCl_3$) δ 7.66 (q, *J* = 8.6 Hz, 4H, Ar), 7.53 (d, *J* = 8.8 Hz, 2H, Ar), 6.99 (d, *J* = 8.6 Hz, 2H, Ar), 4.01 (t, *J* = 6.5 Hz, 2H, ArO$\underline{CH_2}(CH_2)_8CH_2Br$), 3.41 (t, *J* = 6.9 Hz, 2H, ArO$CH_2(CH_2)_8\underline{CH_2}Br$), 1.91 – 1.75 (m, 4H, ArO$CH_2\underline{CH_2}(CH_2)_6\underline{CH_2}CH_2Br$), 1.53 – 1.27 (m, 12H, ArO$CH_2CH_2(\underline{CH_2})_6CH_2CH_2Br$).

^{13}C NMR (101 MHz, $CDCl_3$) δ 159.82, 145.30, 132.58, 131.27, 128.34, 127.09, 119.14, 115.10, 110.06, 68.16, 34.06, 32.83, 29.45, 29.37, 29.33, 29.23, 28.75, 28.17, 26.03.

IR $\bar{\nu}$ cm^{-1}: 2920,2852(aromatic CH), 2235 (C≡N), 1605 (para di-substituted benzene).

4-{4-[(11-Bromoundecyl)oxy]phenyl}benzonitrile

MP = 67 °C T_{NI} = 70 °C

^{1}H NMR (400 MHz, $CDCl_3$) δ 7.68 (q, *J* = 8.6 Hz, 4H,Ar), 7.55 (d, *J* = 8.5 Hz, 2H, Ar), 7.02 (d, *J* = 8.7 Hz, 2H, Ar), 4.03 (t, *J* = 6.5 Hz, 2H, ArO$\underline{CH_2}(CH_2)_9CH_2Br$), 3.43 (t, *J* = 6.9 Hz, 2H, ArO$CH_2(CH_2)_9\underline{CH_2}Br$), 1.94 – 1.78 (m, 4H, ArO$CH_2\underline{CH_2}(CH_2)_7\underline{CH_2}CH_2Br$), 1.59 – 1.15 (m, 14H, ArO$CH_2CH_2(\underline{CH_2})_7CH_2CH_2Br$).

^{13}C NMR (101 MHz, $CDCl_3$) δ 159.83, 145.29, 132.58, 131.25, 128.33, 127.08, 119.14, 115.11, 110.05, 68.18, 34.08, 32.85, 29.53, 29.47, 29.43, 29.38, 29.24, 28.78, 28.19, 26.05.

IR $\bar{\nu}$ cm-1: 2923,2851(aromatic CH), 2224 (C≡N), 1601 (para di-substituted benzene).

4-{4-[(12-Bromododecyl)oxy]phenyl}benzonitrile

MP = 78 °C T_{NI} = 73 °C

^{1}H NMR (400 MHz, $CDCl_3$) δ 7.69 (q, *J* = 8.6 Hz, 4H), 7.55 (d, *J* = 8.7 Hz, 2H), 7.02 (d, *J* = 8.7 Hz, 2H), 4.03 (t, *J* = 6.6 Hz, 2H, ArO$\underline{CH_2}(CH_2)_{10}CH_2Br$), 3.43 (t, *J* = 6.9 Hz, 2H, ArO$CH_2(CH_2)_{10}\underline{CH_2}Br$),

1.94 – 1.78 (m, 4H, $ArOCH_2\underline{CH_2}(CH_2)_8\underline{CH_2}CH_2Br$), 1.55 – 1.22 (m, 16H, $ArOCH_2CH_2(\underline{CH_2})_8CH_2CH_2Br$).

^{13}C NMR (101 MHz, $CDCl_3$) δ 159.83, 145.31, 132.58, 131.27, 128.33, 127.09, 119.14, 115.10, 110.06, 68.19, 34.08, 32.85, 29.55, 29.54, 29.52, 29.44, 29.39, 29.24, 28.78, 28.19, 26.05.

IR $\bar{\nu}$ cm^{-1}: 2919,2851(aromatic CH), 2239 (C≡N), 1605 (para di-substituted benzene).

2.1.2 4-[4-[ω-(4-Formyl-2-nitrophenoxy)alkyloxy]phenyl]benzonitriles

The 4-[4-[ω-(4-formyl-2-nitrophenoxy)alkyloxy]phenyl]benzonitriles were prepared as described elsewhere [1]. 4-{4-[(ω-Bromoalkyl)oxy]phenyl}benzonitrile (1eq) was dissolved in DMF (5 mL) and potassium carbonate (4 eq.) and 4-hydroxy-3-nitrobenzaldehyde (1.2 eq) added. The reaction mixture was heated with stirring overnight at 110 °C. The reaction mixture was allowed to cool, water (70 mL) added, and the precipitate collected. The precipitate was purified by column chromatography with a mix of 3:1 petroleum ether/ethyl acetate as eluent (Rf=0.6). Yields in the range of 45-50 % were obtained as yellow/pale yellow solids.

4-[4-[3-(4-Formyl-2-nitrophenoxy)propyloxy]phenyl]benzonitrile

MP = 160 °C

^1H NMR (400 MHz, $CDCl_3$) δ 9.93 (s, 1H, ArC=O$\underline{H}$), 8.35 (d, *J* = 2.1 Hz, 1H, Ar), 8.07 (dd, *J* = 8.7, 2.1 Hz, 1H, Ar), 7.65 (q, *J* = 8.0 Hz, 4H, Ar), 7.53 (d, *J* = 8.6 Hz, 2H, Ar), 7.26 (d, *J* = 8.7 Hz, 1H, Ar), 7.01 (d, *J* = 8.6 Hz, 2H, Ar), 4.44 (t, J = 5.8 Hz, 2H, $ArOCH_2CH_2\underline{CH_2}ONO_2Ar$), 4.27 (t, *J* = 5.8 Hz, 2H, $ArO\underline{CH_2}CH_2CH_2ONO_2Ar$), 2.39 (p, J = 5.8 Hz, 2H, $ArOCH_2\underline{CH_2}CH_2ONO_2Ar$)).

^{13}C NMR (101 MHz, $CDCl_3$) δ 188.77, 159.48, 156.50, 145.11, 139.86, 134.76, 132.59, 131.58, 129.06, 128.45, 127.49, 127.13, 119.12, 115.11, 114.60, 110.15, 66.56, 65.70, 28.87.

IR $\bar{\nu}$ cm-1: 2920,2852(aromatic CH), 2237 (C≡N), 1696(C=O).

4-[4-[4-(4-Formyl-2-nitrophenoxy)butyloxy]phenyl]benzonitrile

T_{Cr} = 39°C; T_{NI} = 66 °C

^1H NMR (400 MHz, $CDCl_3$) δ 9.93 (s, 1H, ArC=O$\underline{H}$), 8.34 (d, *J* = 2.1 Hz, 1H, Ar), 8.07 (dd, *J* = 8.7, 2.1 Hz, 1H, Ar), 7.67 (d, *J* = 8.3 Hz, 4H, Ar), 7.53 (d, *J* = 8.5 Hz, 2H, Ar), 7.23 (d, *J* = 8.7 Hz, 1H, Ar), 6.99 (d, *J* = 8.7 Hz, 2H, Ar), 4.32 (t, *J* = 5.7 Hz, 2H, , $ArOCH_2(CH_2)_2\underline{CH_2}ONO_2Ar$), 4.09 (t, *J* = 5.9 Hz, 2H, $ArO\underline{CH_2}(CH_2)_2CH_2ONO_2Ar$), 2.18 – 2.01 (m, 4H, $ArOCH_2\underline{CH_2}\underline{CH_2}CH_2ONO_2Ar$).

^{13}C NMR (101 MHz, $CDCl_3$) δ 188.74, 159.46, 156.59, 145.19, 139.94, 134.63, 132.59, 131.57, 128.95, 128.40, 127.50, 127.11, 119.11, 115.05, 114.48, 110.14, 69.91, 67.38, 25.76, 25.75.

IR $\bar{\nu}$ cm^{-1}: 2920,2852(aromatic CH), 2239 (C≡N), 1694 (C=O).

4-[4-[5-(4-Formyl-2-nitrophenoxy)pentyloxy]phenyl]benzonitrile

T_{Cr} = 39°C; T_{NI} = 65 °C

^{1}H NMR (400 MHz, $CDCl_3$) δ 9.92 (s, 1H, ArC=O<u>H</u>), 8.33 (d, *J* = 2.1 Hz, 1H, Ar), 8.06 (d, *J* = 8.6, 2.2 Hz, 1H, Ar), 7.67 (q, J = 8.0 Hz, 4H, Ar), 7.52 (d, *J* = 7.7 Hz, 2H), 7.21 (d, *J* = 8.6 Hz, 1H,Ar), 6.99 (dd, *J* = 8.8, Hz, 2H, Ar), 4.23 (t, *J* = 6.2 Hz, 2H, ArOCH$_2$CH$_2$CH$_2$CH$_2$<u>CH$_2$</u>ONO$_2$Ar), 4.03 (d, *J* = 6.4 Hz, 2H ArO<u>CH$_2$</u>CH$_2$CH$_2$CH$_2$CH$_2$ONO$_2$Ar), 1.98 – 1.81 (m, 4H, ArOCH$_2$<u>CH$_2$</u>CH$_2$<u>CH$_2$</u>CH$_2$ONO$_2$Ar), 1.64 – 1.55 (m, 2H , ArOCH$_2$CH$_2$<u>CH$_2$</u>CH$_2$CH$_2$ONO$_2$Ar).

^{13}C NMR (101 MHz, $CDCl_3$) δ 188.75, 159.72, 156.71, 145.26, 140.00, 134.54, 132.59, 131.37, 128.84, 128.36, 127.46, 127.09, 119.13, 115.09, 114.46, 110.09, 70.16, 67.85, 28.70, 25.66, 25.57.

IR $\bar{\nu}$ cm^{-1}: 2936,2855 (aromatic CH), 2237 (C≡N), 1698 (C=O).

4-[4-[6-(4-Formyl-2-nitrophenoxy)hexyloxy]phenyl]benzonitrile

T_{Cr} = 39°; T_{NI} = 65 C

1H NMR (400 MHz, $CDCl_3$) δ 9.92 (s, 1H, ArC=O<u>H</u>), 8.33 (d, *J* = 2.1 Hz, 1H, Ar), 8.06 (dd, *J* = 8.7, 2.1 Hz, 1H, Ar), 7.66 (q, *J* = 8.3 Hz, 4H, Ar), 7.52 (d, *J* = 8.7 Hz, 2H, Ar), 7.21 (d, *J* = 8.7 Hz, 1H, Ar), 6.99 (d, *J* = 8.8 Hz, 2H, Ar), 4.23 (t, *J* = 6.2 Hz, 2H, ArOCH$_2$(CH$_2$)$_4$<u>CH$_2$</u>ONO$_2$Ar), 4.03 (t, *J* = 6.4 Hz, 2H, ArO<u>CH$_2$</u>(CH$_2$)$_4$CH$_2$ONO$_2$Ar), 1.98 – 1.81 (m, 4H, ArOCH$_2$<u>CH$_2$</u>CH$_2$CH$_2$<u>CH$_2$</u>CH$_2$ONO$_2$Ar), 1.64 – 1.51 (m, 4H, ArOCH$_2$CH$_2$<u>CH$_2$</u><u>CH$_2$</u>CH$_2$CH$_2$ONO$_2$Ar).

^{13}C NMR (101 MHz, $CDCl_3$) δ 188.79, 159.64, 156.65, 145.23, 139.98, 134.63, 132.58, 131.42, 128.87, 128.37, 127.41, 127.09, 119.14, 115.10, 114.49, 110.07, 70.10, 67.74, 28.77, 28.51, 22.55, 22.39.

IR $\bar{\nu}$ cm^{-1}: 2936,2855 (aromatic CH), 2237 (C≡N), 1698 (C=O).

4-[4-[7-(4-Formyl-2-nitrophenoxy)heptyloxy]phenyl]benzonitrile

MP = 96 °C; T_{NI} = 64 °C

^{1}H NMR (400 MHz, $CDCl_3$) δ 9.93 (s, 1H), 8.33 (d, *J* = 2.1 Hz, 1H, Ar), 8.06 (dd, *J* = 8.8, 2.1 Hz, 1H, Ar), 7.66 (q, *J* = 8.5 Hz, 4H, Ar), 7.53 (d, *J* = 8.7 Hz, 2H, Ar), 7.20 (d, *J* = 8.7 Hz, 1H, Ar), 6.99 (d, *J* = 8.6 Hz, 2H, Ar), 4.22 (t, *J* = 6.3 Hz, 2H, ArOCH$_2$(CH$_2$)$_4$<u>CH$_2$</u>ONO$_2$Ar), 4.02 (t, *J* = 6.5 Hz, 2H, ArO<u>CH$_2$</u>(CH$_2$)$_4$CH$_2$ONO$_2$Ar), 1.94 – 1.76 (m, 4H , ArOCH$_2$<u>CH$_2$</u>CH$_2$CH$_2$CH$_2$<u>CH$_2$</u>CH$_2$ONO$_2$Ar), 1.37 – 1.18 (m, 6H, ArOCH$_2$CH$_2$<u>CH$_2$</u><u>CH$_2$</u><u>CH$_2$</u>CH$_2$CH$_2$ONO$_2$Ar).

^{13}C NMR (101 MHz, $CDCl_3$) δ 188.78, 159.79, 156.74, 145.28, 140.00, 134.54, 132.58, 131.32, 128.80, 128.34, 127.45, 127.09, 119.14, 115.10, 114.47, 110.06, 70.30, 68.10, 29.11, 28.93, 28.69, 25.92, 25.78.

IR $\bar{\nu}$ cm^{-1}: 2936,2855 (aromatic CH), 2237 (C≡N), 1698 (C=O).

4-[4-[8-(4-Formyl-2-nitrophenoxy)octyloxy]phenyl]benzonitrile

T_{Cr} = 35 °C; T_{NI} = 80 °C

^{1}H NMR (400 MHz, $CDCl_3$) δ 9.93 (s, 1H, ArC=O<u>H</u>), 8.33 (d, *J* = 2.1 Hz, 1H, Ar), 8.06 (dd, *J* = 8.7, 2.1 Hz, 1H, Ar), 7.66 (q, *J* = 8.3 Hz, 4H, Ar), 7.53 (d, *J* = 8.6 Hz, 2H, Ar), 7.20 (d, *J* = 8.7 Hz, 1H, Ar), 6.99 (d, *J* = 8.7 Hz, 2H, Ar), 4.21 (t, *J* = 6.3 Hz, 2H, $ArOCH_2(CH_2)_6\underline{CH_2}ONO_2Ar$), 4.01 (t, *J* = 6.5, Hz, 2H, $ArO\underline{CH_2}(CH_2)_6CH_2ONO_2Ar$), 1.94 – 1.75 (m, 4H, $ArOCH_2\underline{CH_2}(CH_2)_4\underline{CH_2}CH_2ONO_2Ar$), 1.46 – 1.34 (m, 8H $ArOCH_2CH_2\underline{(CH_2)_4}CH_2CH_2ONO_2Ar$).

^{13}C NMR (101 MHz, $CDCl_3$) δ 188.76, 159.79, 156.76, 145.29, 140.02, 134.52, 132.58, 131.30, 128.79, 128.34, 127.46, 127.09, 119.14, 115.10, 114.47, 110.07, 70.33, 68.10, 29.21,29.19, 29.11, 28.74, 25.94, 25.73.

IR $\bar{\nu}$ cm^{-1}: 2934,2855 (aromatic CH), 2231 (C≡N), 1698 (C=O).

4-[4-[9-(4-Formyl-2-nitrophenoxy)nonyloxy]phenyl]benzonitrile

T_{Cr} = 38°C; T_{NI} = 58 °C

^{1}H NMR (400 MHz, $CDCl_3$) δ 9.92 (s, 1H, ArC=O<u>H</u>), 8.33 (d, *J* = 2.1 Hz, 1H, Ar), 8.05 (dd, *J* = 8.7, 2.1 Hz, 1H, Ar), 7.67 (q, *J* = 8.4 Hz, 4H, Ar), 7.52 (d, *J* = 8.7 Hz, 2H, Ar), 7.20 (d, *J* = 8.7 Hz, 1H, Ar), 6.99 (d, *J* = 8.8 Hz, 2H, Ar), 4.20 (t, *J* = 6.3 Hz, 2H, $ArOCH_2(CH_2)_7\underline{CH_2}ONO_2Ar$), 4.01 (t, *J* = 6.6, Hz, 2H, $ArO\underline{CH_2}(CH_2)_7CH_2ONO_2Ar$), 1.87 – 1.70 (m, 4H, $ArOCH_2\underline{CH_2}(CH_2)_5\underline{CH_2}CH_2ONO_2Ar$), 1.43– 1.34 (m, 10H, $ArOCH_2CH_2\underline{(CH_2)_5}CH_2CH_2ONO_2Ar$).

^{13}C NMR (101 MHz, $CDCl_3$) δ 188.77, 159.81, 156.77, 145.30, 140.01, 134.52, 132.58, 131.28, 128.77, 128.33, 127.45, 127.09, 119.14, 115.10, 114.47, 110.05, 70.36, 68.13, 29.36, 29.23, 29.20, 29.11, 28.74, 26.00, 25.76.

IR $\bar{\nu}$ cm^{-1}: 2922,2850 (aromatic CH), 2222 (C≡N), 1692 (C=O).

4-[4-[10-(4-Formyl-2-nitrophenoxy)decyloxy]phenyl]benzonitrile

T_{Cr} = 40°C; T_{NI} = 77 °C

^{1}H NMR (400 MHz, $CDCl_3$) δ 9.92 (s, 1H, ArC=O<u>H</u>), 8.33 (d, *J* = 2.1 Hz, 1H, Ar), 8.05 (dd, *J* = 8.7, 2.1 Hz, 1H, Ar), 7.66 (q, *J* = 8.5 Hz, 4H, Ar), 7.52 (d, *J* = 8.6 Hz, 2H, Ar), 7.20 (d, *J* = 8.7 Hz, 1H, Ar), 6.99 (d, *J* = 8.8 Hz, 2H, Ar), 4.20 (t, *J* = 6.3 Hz, 2H, $ArOCH_2(CH_2)_8\underline{CH_2}ONO_2Ar$), 4.00 (t, *J* =

6.6, Hz, 2H, ArO$\underline{CH_2}(CH_2)_8CH_2ONO_2Ar$), 1.93 – 1.75 (m, 5H, $ArOCH_2\underline{CH_2}(CH_2)_6\underline{CH_2}CH_2ONO_2Ar$), 1.46-1.36 (m, 12H, $ArOCH_2CH_2\underline{(CH_2)_6}CH_2CH_2ONO_2Ar$).

^{13}C NMR (101 MHz, $CDCl_3$) δ 188.81, 159.83, 156.78, 145.28, 139.99, 134.58, 132.57, 131.22, 128.75, 128.33, 127.38, 127.07, 119.14, 115.11, 114.50, 110.01, 70.39, 68.17, 29.43, 29.38, 29.34, 29.22, 29.18, 28.75, 26.02, 25.77.

IR $\bar{\nu}$ cm^{-1}: 2928,2855 (aromatic CH), 2233 (C≡N), 1698(C=O).

4-[4-[11-(4-Formyl-2-nitrophenoxy)undecyloxy]phenyl]benzonitrile

T_{Cr} = 56°C; T_{NI} = 63 °C

^1H NMR (400 MHz, $CDCl_3$) δ 9.93 (s, 1H, ArC=O$\underline{H}$), 8.33 (d, *J* = 2.1 Hz, 1H, Ar), 8.05 (d, *J* = 8.9 Hz, 1H, Ar), 7.66 (q, *J* = 8.6 Hz, 4H, Ar), 7.53 (d, *J* = 8.4 Hz, 2H, Ar), 7.20 (d, *J* = 8.7 Hz, 1H, Ar), 6.99 (d, *J* = 8.6 Hz, 2H, Ar), 4.20 (t, *J* = 6.4 Hz, 2H, $ArOCH_2(CH_2)_9\underline{CH_2}ONO_2Ar$), 4.01 (t, *J* = 6.6 Hz, 2H, ArO$\underline{CH_2}(CH_2)_9CH_2ONO_2Ar$), 1.91 – 1.77 (m, 4H, $ArOCH_2\underline{CH_2}(CH_2)_7\underline{CH_2}CH_2ONO_2Ar$), 1.46-1.33 (s, 14H, $ArOCH_2CH_2\underline{(CH_2)_7}CH_2CH_2ONO_2Ar$).

13C NMR (101 MHz, $CDCl_3$) δ 188.78, 159.83, 156.79, 145.30, 140.01, 134.51, 132.58, 131.27, 128.76, 128.33, 127.45, 127.08, 119.14, 115.10, 114.48, 110.05, 70.39, 68.19, 29.52, 29.44, 29.36, 29.23, 29.19, 28.75, 26.04, 25.77, 25.75.

IR $\bar{\nu}$ cm^{-1}: 2920,2852 (aromatic CH), 2235 (C≡N), 1692 (C=O).

4-[4-[12-(4-Formyl-2-nitrophenoxy)dodecyloxy]phenyl]benzonitrile

T_{Cr} = 75°C; T_{NI} = 96 °C

^1H NMR (400 MHz, $CDCl_3$) δ 9.92 (s, 1H, ArC=O$\underline{H}$), 8.32 (d, *J* = 2.1 Hz, 1H, Ar), 8.05 (dd, *J* = 8.7, 2.1 Hz, 1H, Ar), 7.66 (q, *J* = 8.3 Hz, 4H, Ar), 7.52 (d, *J* = 8.6 Hz, 2H, Ar), 7.20 (d, *J* = 8.7 Hz, 1H, Ar), 6.98 (d, *J* = 8.9 Hz, 2H, Ar), 4.20 (t, *J* = 6.4 Hz, 2H, $ArOCH_2(CH_2)_{10}\underline{CH_2}ONO_2Ar$), 4.00 (t, *J* = 6.5 Hz, 2H, ArO$\underline{CH_2}(CH_2)_{10}CH_2ONO_2Ar$), 1.92 – 1.74 (m, 4H, $ArOCH_2\underline{CH_2}(CH_2)_8\underline{CH_2}CH_2ONO_2Ar$), 1.51-1.31 (m, 16H, $ArOCH_2CH_2\underline{(CH_2)_8}CH_2CH_2ONO_2Ar$).

^{13}C NMR (101 MHz, $CDCl_3$) δ 188.78, 159.82, 156.79, 145.30, 140.00, 134.51, 132.57, 131.25, 128.75, 128.32, 127.43, 127.08, 119.13, 115.10, 114.48, 110.04, 70.39, 68.19, 29.54, 29.51, 29.45, 29.38, 29.23, 29.20, 28.75, 26.03, 25.77.

IR $\bar{\nu}$ cm^{-1}: 2917,2851 (aromatic CH), 2232 (C≡N), 1685(C=O).

2.1.3. (4-Nitrophenyl) 2,4-dimethoxybenzoate

2,4-Dimethoxybenzoic acid (1.00 g, 5.48 mmol) and DCC (1.69 g, 8.23 mmol) were dissolved in DCM (50 mL) and after 5 min, 4-nitrophenol (0.91 g, 6.58 mmol) was added. After a further 30 min,

DMAP (0.10g, 0.82 mmol) was added. The reaction was left overnight with stirring at room temperature. The reaction solution was concentrated, and the crude product recrystalized in ethanol (100 mL). Yield = 69.7 %.

MP = 115 °C

^{1}H NMR (400 MHz, $CDCl_3$) δ 8.29 (d, *J* = 9.0 Hz, 2H, Ar), 8.07 (d, *J* = 8.7 Hz, 1H, Ar), 7.39 (d, *J* = 9.2 Hz, 2H, Ar), 6.61 – 6.52 (m, 2H, Ar), 3.93 (s, 3H Ar-O$\underline{CH_3}$), 3.90 (s, 3H, Ar-O$\underline{CH_3}$).

^{13}C NMR (101 MHz, $CDCl_3$) δ 165.58, 162.65, 162.49, 156.11, 145.11, 134.70, 125.12, 122.81, 109.99, 105.09, 99.03, 56.06, 55.67.

IR $\bar{\nu}$ cm^{-1}: 3113, 2986 (b, aromatic CH), 1707(C=O).

2.1.4 (4-Aminophenyl) 2,4-dimethoxybenzoate

To a pre-dried flask flushed with argon, 4-nitrophenyl 2,4-dimethoxybenzoate (1.00 g, 3.29 mmol) was dissolved in DCM (50 mL). The mixture was sparged with argon and 5% Pd/C catalyst (0.017 g, 0.165 mmol) was added. The argon atmosphere was evacuated under vacuum and replaced by hydrogen gas. The reaction was allowed to proceed for 4 h at room temperature. The hydrogen gas was evacuated under vacuum and the flask purged using argon. The mixture was filtered through Celite, and the collected solvent was evaporated under vacuum to leave a brown solid which was carried forwards without any further purification. Yield = 88.6 %.

MP = 172 °C

^{1}H NMR (400 MHz, $CDCl_3$) δ 8.04 (d, *J* = 8.7 Hz, 1H, Ar), 6.98 (d, *J* = 8.6 Hz, 2H, Ar), 6.69 (d, *J* = 8.6 Hz, 2H, Ar), 6.58 – 6.49 (m, 2H, Ar), 3.91 (s, 3H, Ar-O$\underline{CH_3}$), 3.88 (s, 3H, Ar-O$\underline{CH_3}$), 3.62 (s, 2H Ar-$\underline{NH_2}$).

^{13}C NMR (101 MHz, $CDCl_3$) δ 164.73, 164.34, 162.04, 143.91, 143.31, 134.37, 122.56, 115.65, 111.70, 104.71, 99.07, 56.04, 55.56.

IR $\bar{\nu}$ cm^{-1}: 3458 (N-H, primary amine) 3016, 2918 (b, aromatic CH), 1718(C=O).

*2.1.5 [4[(E)-[4-[4-[ω-(4-cyanophenyl)phenoxy]alkyloxy]-3-nitrophenyl]methylideneamino]phenyl] 2,4-dimethoxybenzoates, **1**-n*

4-[4-[4-(4-formyl-2-nitrophenoxy)alkyloxy]phenyl]benzonitrile (1 eq.) was solubilized in ethanol, the appropriate 4-aminophenyl 3,4-dimethoxybenzoate (1,2 eq.) was added and the reaction mixture heated at reflux with stirring for 4 h. The mixture was cooled to room temperature and the resulting precipitate collected by vacuum filtration. The crude product was recrystallized from ethanol to give the title compound as a solid. The yield was between 38-40%.

1-3

^{1}H NMR (400 MHz, $CDCl_3$) δ 8.43 (s, 1H, N=<u>CH</u>), 8.38 (d, *J* = 2.0 Hz, 1H, Ar), 8.08 (d, J = 8.7 Hz, 2H, Ar), 7.66 (q, *J* = 8.1 Hz, 4H, Ar), 7.53 (d, *J* = 8.5 Hz, 2H, Ar), 7.26 (m, 4H, Ar), 7.21 (d, *J* = 8.9 Hz, 1H, Ar), 7.03 (d, *J* = 8.4 Hz, 2H, Ar), 6.60 – 6.52 (m, 2H, Ar), 4.41 (t, *J* = 5.8 Hz, 2H, $ArOCH_2CH_2\underline{CH_2}ONO_2Ar$), 4.29 (t, *J* = 5.9 Hz, 2H, $ArO\underline{CH_2}CH_2CH_2ONO_2Ar$), 3.93 (s, 3H, Ar-$O\underline{CH_3}$), 3.90 (s, 3H, Ar-$O\underline{CH_3}$), 2.42 – 2.35 (m, 2H $ArOCH_2\underline{CH_2}CH_2ONO_2Ar$).

^{13}C NMR (101 MHz, $CDCl_3$) δ 165.04, 163.70, 162.28, 159.34, 156.65, 154.15, 149.68, 148.46, 145.20, 139.96, 134.52, 133.80, 132.60, 131.77, 129.21, 128.45, 127.15, 126.06, 122.78, 121.73, 119.09, 115.14, 114.45, 111.14, 110.17, 104.84, 99.07, 66.19, 63.92, 56.06, 55.61, 29.00.

IR $\bar{\nu}$ cm^{-1}: 2919 (b, aromatic CH), 2225 (C≡N), 1793(C=O).

MS (ESI+, m/z) = $[M+Na]^+$: Calculated for $C_{38}H_{31}N_3O_8Na$: 680.2009 Found: 680.1985.

1-4

^{1}H NMR (400 MHz, $CDCl_3$) δ 8.45 (s, 1H, N=<u>CH</u>), 8.39 (d, *J* = 2.1 Hz, 1H, Ar), 8.08 (d, J = 8.7 Hz, 2H, Ar), 7.70 (q, *J* = 8.3 Hz, 4H, Ar), 7.56 (d, *J* = 8.6 Hz, 2H, Ar), 7.32 - 7.22 (m, 4H, Ar), 7.20 (d, *J* = 8.8 Hz, 1H, Ar), 7.02 (d, J = 8.8 Hz, 2H, Ar), 6.63 – 6.54 (m, 2H, Ar), 4.31 (t, *J* = 5.5 Hz, 2H, $ArOCH_2(CH_2)_2\underline{CH_2}ONO_2Ar$), 4.15 (t, *J* = 5.6 Hz, 2H, $ArO\underline{CH_2}(CH_2)_2CH_2ONO_2Ar$), 3.96 (s, 3H, Ar-$O\underline{CH_3}$), 3.92 (s, 3H, Ar-$O\underline{CH_3}$), 2.20 – 2.04 (m, H $ArOCH_2\underline{(CH_2)_2}CH_2ONO_2Ar$).

^{13}C NMR (101 MHz, $CDCl_3$) δ 165.04, 163.75, 162.28, 159.53, 156.70, 154.24, 149.67, 148.49, 145.25, 140.01, 134.52, 133.73, 132.59, 131.52, 129.05, 128.40, 127.12, 126.02, 122.78, 121.73, 119.13, 115.08, 114.37, 111.14, 110.11, 104.85, 99.07, 69.53, 67.47, 56.07, 55.61, 25.84, 25.80.

IR $\bar{\nu}$ cm^{-1}: 2917 (b, aromatic CH), 2225 (C≡N), 1735(C=O).

MS (ESI+, m/z) = $[M+Na]^+$: Calculated for $C_{39}H_{33}N_3O_8Na$: 694.2165 Found: 694.2155.

1-5

^{1}H NMR (400 MHz, $CDCl_3$) δ 8.45 (s, 1H, N=<u>CH</u>), 8.38 (d, *J* = 2.1 Hz, 1H, Ar), 8.11 (d, *J* = 8.7 Hz, 2H, Ar), 7.69 (q, *J* = 8.2 Hz, 4H, Ar), 7.55 (d, *J* = 8.1 Hz, 2H, Ar), 7.32 – 7.23 (m, 4H, Ar), 7.03 (d, *J* = 8.2 Hz, 2H, Ar), 6.63 – 6.54 (m, 2H, Ar), 4.25 (t, *J* = 6.0 Hz, 2H, $ArOCH_2(CH_2)_3\underline{CH_2}ONO_2Ar$), 4.09 (t, *J* = 6.1 Hz, 2H, $ArO\underline{CH_2}(CH_2)_3CH_2ONO_2Ar$), 3.96 (s, 3H, Ar-$O\underline{CH_3}$), 3.92 (s, 3H, Ar-$O\underline{CH_3}$), 2.04 – 1.88 (m, 4H, $ArOCH_2\underline{CH_2}CH_2\underline{CH_2}CH_2ONO_2Ar$), 1.81 – 1.72 (m, 2H, $ArOCH_2CH_2\underline{CH_2}CH_2CH_2ONO_2Ar$).

^{13}C NMR (101 MHz, $CDCl_3$) δ 165.04, 163.75, 162.28, 159.67, 156.74, 154.30, 149.65, 148.51, 145.28, 140.08, 134.52, 133.68, 132.58, 131.42, 128.97, 128.37, 127.11, 125.96, 122.77, 121.73,

119.14, 115.12, 114.39, 111.15, 110.07, 104.85, 99.07, 69.74, 67.80, 56.07, 55.61, 28.81, 28.62, 22.58.

IR $\bar{\nu}$ cm^{-1}: 2918 (b, aromatic CH), 2225 (C≡N), 1732(C=O).

MS (ESI+, m/z) = $[M+Na]^+$: Calculated for $C_{40}H_{35}N_3O_8Na$: 708.2322 Found: 708.2310.

1-6

^{1}H NMR (400 MHz, $CDCl_3$) δ 8.42 (s, 1H, N=<u>CH</u>), 8.35 (d, *J* = 2.1 Hz, 1H, Ar), 8.08 (dd, J = 8.8, 2.7 Hz, 2H, Ar), 7.66 (q, *J* = 8.4 Hz, 4H, Ar), 7.53 (d, *J* = 8.7 Hz, 2H), 7.27 – 7.20 (m, 4H, Ar), 7.16 (d, *J* = 8.8 Hz, 1H, Ar), 7.00 (d, *J* = 8.8 Hz, 2H, Ar), 6.61 – 6.52 (m, 2H, Ar), 4.21 (t, *J* = 6.2 Hz, 2H, $ArOCH_2(CH_2)_4\underline{CH_2}ONO_2Ar$), 4.04 (t, *J* = 6.4 Hz, 2H, $ArO\underline{CH_2}(CH_2)_4CH_2ONO_2Ar$), 3.93 (s, 3H, Ar-O<u>CH$_3$</u>), 3.90 (s, 3H, Ar-O<u>CH$_3$</u>), 1.96 – 1.83 (m, 4H, $ArOCH_2\underline{CH_2}CH_2CH_2\underline{CH_2}CH_2ONO_2Ar$), 1.66 – 1.58 (m, 4H, $ArOCH_2CH_2\underline{CH_2CH_2}CH_2CH_2ONO_2Ar$)

^{13}C NMR (101 MHz, CDCl3) δ 165.04, 163.76, 162.27, 159.75, 156.77, 154.37, 149.64, 148.52, 145.30, 140.06, 134.52, 133.65, 132.58, 131.34, 128.89, 128.35, 127.10, 125.98, 122.77, 121.72, 119.14, 115.11, 114.39, 111.15, 110.05, 104.85, 99.07, 69.80, 67.88, 56.06, 55.61, 29.07, 28.80, 25.66, 25.60.

IR $\bar{\nu}$ cm^{-1}: 2938 (b, aromatic CH), 2218 (C≡N), 1732(C=O).

EA for $C_{41}H_{37}N_3O_8$ Calculated: C= 70.37 % H = 5.33 % N = 6.01 % Found: C= 70.36 % H = 5.73 % N = 5.33 %.

1-7

^{1}H NMR (400 MHz, $CDCl_3$) δ 8.45 (s, 1H, N=<u>CH</u>), 8.38 (d, *J* = 2.1 Hz, 1H, Ar), 8.10 (dd, *J* = 8.7, 2.7 Hz, 1H), 7.69 (q, *J* = 8.6 Hz, 4H, Ar), 7.55 (d, J = 8.3 Hz, 2H, Ar), 7.32 – 7.21 (m, 4H, Ar), 7.02 (d, *J* = 8.7 Hz, 2H, Ar), 6.63 – 6.54 (m, 2H, Ar), 4.22 (t, *J* = 6.3 Hz, 2H, $ArOCH_2(CH_2)_5\underline{CH_2}ONO_2Ar$), 4.05 (t, *J* = 6.4 Hz, 2H, $ArO\underline{CH_2}(CH_2)_5CH_2ONO_2Ar$), 3.96 (s, 3H, Ar-O<u>CH$_3$</u>), 3.92 (s, 3H, Ar-O<u>CH$_3$</u>), 1.98 – 1.81 (m, 4H $ArOCH_2\underline{CH_2}CH_2CH_2CH_2\underline{CH_2}CH_2ONO_2Ar$), 1.65 – 1.45 (m, 6H, $ArOCH_2CH_2\underline{CH_2CH_2CH_2}CH_2CH_2ONO_2Ar$).

^{13}C NMR (101 MHz, $CDCl_3$) δ 165.04, 163.75, 162.27, 159.79, 156.78, 154.39, 149.64, 148.53, 145.30, 140.08, 134.52, 133.65, 132.58, 131.29, 128.86, 128.34, 127.09, 125.95, 122.77, 121.72, 119.15, 115.11, 114.39, 111.15, 110.04, 104.85, 99.07, 69.94, 68.05, 56.07, 55.61, 29.11, 28.96, 28.79, 25.93, 25.82.

IR $\bar{\nu}$ cm^{-1}: 2938 (b, aromatic CH), 2222 (C≡N), 1738(C=O).

MS (ESI+, m/z) = $[M+Na]^+$: Calculated for $C_{42}H_{39}N_3O_8Na$: 736.2635 Found: 736.2613.

1-8

^{1}H NMR (400 MHz, $CDCl_3$) δ 8.42 (s, 1H, N=<u>CH</u>), 8.35 (d, *J* = 2.1 Hz, 1H, Ar), 8.08 (dd, *J* = 8.7, 2.8 Hz, 2H, Ar), 7.66 (q, *J* = 8.3 Hz, 4H, Ar), 7.53 (d, *J* = 8.7 Hz, 2H, Ar), 7.28 – 7.23 (m, 4H, Ar), 7.16 (d, *J* = 8.8 Hz, 1H, Ar), 7.00 (dd, *J* = 8.7 Hz, 2H,), 6.61 – 6.50 (m, 2H, Ar), 4.19 (t, *J* = 6.3 Hz, 2H, $ArOCH_2(CH_2)_6\underline{CH_2}ONO_2Ar$), 4.02 (t, *J* = 6.5 Hz, 2H, $ArO\underline{CH_2}(CH_2)_6CH_2ONO_2Ar$), 3.93 (s, 3H, Ar-O<u>CH$_3$</u>), 3.90 (s, 3H, Ar-O<u>CH$_3$</u>), 1.94 – 1.77 (m, 4H, $ArOCH_2\underline{CH_2}(CH_2)_4\underline{CH_2}CH_2ONO_2Ar$), 1.55 – 1.39 (m, 8H, $ArOCH_2CH_2\underline{(CH_2)_4}CH_2CH_2ONO_2Ar$)

^{13}C NMR (101 MHz, $CDCl_3$) δ 165.04, 163.76, 162.27, 159.81, 156.81, 154.42, 149.63, 148.54, 145.32, 140.07, 134.52, 133.63, 132.58, 131.28, 128.83, 128.34, 127.09, 125.97, 122.76, 121.72, 119.15, 115.12, 114.40, 111.15, 110.03, 104.85, 99.07, 69.97, 68.13, 56.06, 55.61, 29.20, 29.18, 29.14, 28.85, 25.93, 25.77.

IR $\bar{\nu}$ cm^{-1}: 2945 (b, aromatic CH), 2225 (C≡N), 1736(C=O).

EA for $C_{43}H_{41}N_2O$ Calculated: C= 70.96 % H = 5.68 % N = 5.77 % Found: C= 70.70 % H = 5.65 % N = 5.66 %.

1-9

^{1}H NMR (400 MHz, $CDCl_3$) δ 8.43 (s, 1H, N=<u>CH</u>), 8.36 (d, *J* = 2.1 Hz, 1H, Ar), 8.09 (dd, J = 8.8 2.8 Hz, 2H)7.68 (q, *J* = 8.7 Hz, 4H, Ar), 7.54 (d, *J* = 8.7 Hz, 2H, Ar), 7.30 – 7.25 (m, 4H, Ar), 7.17 (d, *J* = 8.7 Hz, 1H, Ar), 7.00 (d, *J* = 8.6 Hz, 2H, Ar), 6.62 – 6.53 (m, 2H, Ar), 4.20 (t, *J* = 6.4 Hz, 2H, $ArOCH_2(CH_2)_7\underline{CH_2}ONO_2Ar$), 4.03 (t, *J* = 6.5 Hz, 2H, $ArO\underline{CH_2}(CH_2)_7CH_2ONO_2Ar$), 3.95 (s, 3H, Ar-O<u>CH$_3$</u>), 3.91 (s, 3H, Ar-O<u>CH$_3$</u>), 1.94 – 1.78 (m, 4H, $ArOCH_2\underline{CH_2}(CH_2)_5\underline{CH_2}CH_2ONO_2Ar$), 1.55 – 1.35 (m, 10H, $ArOCH_2CH_2\underline{(CH_2)_5}CH_2CH_2ONO_2Ar$).

^{13}C NMR (101 MHz, $CDCl_3$) δ 165.04, 163.75, 162.27, 159.83, 156.81, 154.43, 149.63, 148.54, 145.31, 140.08, 134.52, 133.64, 132.58, 131.25, 128.82, 128.33, 127.09, 125.95, 122.76, 121.72, 119.15, 115.11, 114.40, 111.15, 110.03, 104.85, 99.07, 70.00, 68.16, 56.06, 55.61, 29.37, 29.23, 29.21, 29.13, 28.85, 26.00, 25.79.

IR $\bar{\nu}$ cm^{-1}: 2935 (b, aromatic CH), 2218 (C≡N), 1736(C=O)

MS (ESI+, m/z) = $[M+Na]^+$: Calculated for $C_{44}H_{43}N_3O_8Na$: 764.2948 Found: 764.2961.

1-10

^{1}H NMR (400 MHz, $CDCl_3$) δ 8.42 (s, 1H, N=<u>CH</u>), 8.35 (d, *J* = 2.1 Hz, 1H, Ar), 8.08 (dd, *J* = 8.7 2.1 Hz, 2H), 7.66 (q, *J* = 8.2 Hz, 4H), 7.52 (d, *J* = 8.7 Hz, 2H, Ar), 7.27 – 7.19 (m, 4H, Ar), 7.15 (d, *J* = 8.8 Hz, 1H, Ar), 6.99 (d, *J* = 8.8 Hz, 2H, Ar), 6.61 – 6.50 (m, 2H, Ar), 4.18 (t, *J* = 6.4 Hz, 2H, $ArOCH_2(CH_2)_8\underline{CH_2}ONO_2Ar$), 4.01 (t, J = 6.5 Hz, 2H, $ArO\underline{CH_2}(CH_2)_8CH_2ONO_2Ar$), 3.93 (s, 3H, Ar-

O<u>CH$_3$</u>), 3.90 (s, 3H, Ar-O<u>CH$_3$</u>), 1.93 – 1.76 (m, 4H, ArOCH$_2$<u>CH$_2$</u>(CH$_2$)$_6$<u>CH$_2$</u>CH$_2$ONO$_2$Ar), 1.60 – 1.29 (m, 12H, ArOCH$_2$CH$_2$<u>(CH$_2$)$_6$</u>CH$_2$CH$_2$ONO$_2$Ar).

^{13}C NMR (101 MHz, CDCl$_3$) δ 165.04, 163.76, 162.27, 159.83, 156.83, 154.41, 149.62, 148.55, 145.32, 140.03, 134.52, 133.62, 132.58, 131.26, 128.80, 128.33, 127.09, 125.97, 122.76, 121.72, 119.15, 115.11, 114.41, 111.15, 110.03, 104.84, 99.07, 70.02, 68.18, 56.06, 55.61, 29.43, 29.39, 29.33, 29.22, 29.20 28.86, 26.01, 25.81.

IR $\bar{\nu}$ cm^{-1}: 2921 (b, aromatic CH), 2225 (C≡N), 1736(C=O).

MS (ESI+, m/z) = [M+Na]$^+$: Calculated for $C_{45}H_{45}N_3O_8Na$: 778.3104 Found: 778.3108.

1-11

^{1}H NMR (400 MHz, CDCl$_3$) δ 8.44 (s, 1H, N=<u>CH</u>), 8.37 (d, *J* = 2.1 Hz, 1H, Ar), 8.10 (d, J = 8.6 Hz, 2H), 7.69 (d, *J* = 8.0 Hz, 4H, Ar), 7.55 (d, *J* = 6.9 Hz, 2H, Ar), 7.31 – 7.23 (m, 4H, Ar), 7.18 (d, *J* = 8.8 Hz, 1H, Ar), 7.01 (d, J = 8.8 Hz, 2H, Ar), 6.63 – 6.52 (m, 2H, Ar), 4.20 (t, *J* = 6.4 Hz, 2H. ArOCH$_2$(CH$_2$)$_9$<u>CH$_2$</u>ONO$_2$Ar), 4.03 (t, *J* = 6.6 Hz, 2H, ArO<u>CH$_2$</u>(CH$_2$)$_9$CH$_2$ONO$_2$Ar), 3.96 (s, 3H, Ar-O<u>CH$_3$</u>), 3.92 (s, 3H, Ar-O<u>CH$_3$</u>), 1.95 – 1.78 (m, 4H, ArOCH$_2$<u>CH$_2$</u>(CH$_2$)$_7$<u>CH$_2$</u>CH$_2$ONO$_2$Ar), 1.57 – 1.30 (m, 14H, ArOCH$_2$CH$_2$<u>(CH$_2$)$_7$</u>CH$_2$CH$_2$ONO$_2$Ar).

^{13}C NMR (101 MHz, CDCl$_3$) δ 165.03, 163.75, 162.27, 159.84, 156.82, 154.45, 149.62, 148.55, 145.32, 140.07, 134.52, 133.63, 132.58, 131.25, 128.80, 128.33, 127.08, 125.95, 122.76, 121.72, 119.15, 115.11, 114.41, 111.16, 110.03, 104.85, 99.07, 70.03, 68.20, 56.06, 55.61, 29.52, 29.44, 29.36, 29.28, 29.23, 29.21, 28.87, 26.03, 25.81.

IR $\bar{\nu}$ cm^{-1}: 2918 (b, aromatic CH), 2225 (C≡N), 1736(C=O).

MS (ESI+, m/z) = [M+Na]$^+$: Calculated for $C_{46}H_{47}N_3O_8Na$: 792.3261 Found: 792.3275.

1-12

^{1}H NMR (400 MHz, CDCl$_3$) δ 8.42 (s, 1H, N=<u>CH</u>), 8.35 (d, *J* = 2.1 Hz, 1H, Ar), 8.08 (d, *J* = 8.6 Hz, 2H)7.66 (q, *J* = 8.4 Hz, 4H, Ar), 7.52 (d, *J* = 8.8 Hz, 2H, Ar), 7.27 – 7.20 (m, 4H, Ar), 7.15 (d, *J* = 8.8 Hz, 1H, Ar), 6.99 (d, *J* = 8.8 Hz, 2H, Ar), 6.61 – 6.52 (m, 2H, Ar), 4.18 (t, *J* = 6.4 Hz, 2H), 4.01 (t, J = 6.6 Hz, 2H), 3.93 (s, 3H), 3.90 (s, 3H), 1.92 – 1.75 (m, 4H), 1.59 – 1.24 (m, 16H).

^{13}C NMR (101 MHz, CDCl$_3$) δ 165.03, 163.76, 162.27, 159.84, 156.83, 154.46, 149.62, 148.56, 145.32, 140.08, 134.52, 133.62, 132.58, 131.25, 128.79, 128.33, 127.09, 125.97, 122.76, 121.72, 119.15, 115.11, 114.41, 111.16, 110.03, 104.84, 99.07, 70.04, 68.20, 56.06, 55.61, 29.55, 29.51, 29.47, 29.38, 29.24, 28.87, 26.04, 25.82.

IR $\bar{\nu}$ cm^{-1}: 2928 (b, aromatic CH), 2225 (C≡N), 1735(C=O).

MS (ESI+, m/z) = [M+Na]$^+$: Calculated for $C_{47}H_{49}N_3O_8Na$: 806.3417 Found: 806.3430.

2.2 [4[(E)-[4-[3-[ω-(4-cyanophenyl)phenoxy]alkyloxy]-4-nitrophenyl]methylideneamino]phenyl] 2,4-dimethoxybenzoates, 2-n series

The synthesis of the **2**-*n* dimers used essentially the identical route shown in Scheme ES1 except that 3-hydroxy-4-nitrobenzaldehyde was used in place of 4-hydroxy-3-nitrobenzaldehyde.

2.2.1 4-[4-[ω-(3-formyl-2-nitrophenoxy)alkyloxy]phenyl]benzonitriles

The 4-[4-[ω-(3-formyl-2-nitrophenoxy)alkyloxy]phenyl]benzonitriles were prepared using the method described in 2.1.2 except that 3-hydroxy-4-nitrobenzaldehyde was used in place 4-hydroxy-3-nitrobenzaldehyde, acetonitrile replaced DMF as the reaction solvent.

4-[4-[5-(3-formyl-2-nitrophenoxy)pentyloxy]phenyl]benzonitrile

MP = 120 °C

^{1}H NMR (400 MHz, $CDCl_3$) δ 10.04 (s, 1H, ArC=OH), 7.91 (d, *J* = 8.1 Hz, 1H, Ar), 7.66 (q, *J* = 8.5 Hz, 4H), 7.58 (d, *J* = 1.5 Hz, 1H, Ar), 7.55 – 7.49 (m, 3H, Ar), 6.99 (d, *J* = 8.8 Hz, 2H, Ar), 4.23 (t, *J* = 6.2 Hz, 2H, $ArOCH_2(CH_2)_3\underline{CH_2}ONO_2Ar$), 4.06 (t, *J* = 6.3 Hz, 2H, $ArO\underline{CH_2}(CH_2)_3CH_2ONO_2Ar$), 2.02 – 1.85 (m, 4H, $ArOCH_2\underline{CH_2}CH_2\underline{CH_2}CH_2ONO_2Ar$), 1.72 (m, 2H, $ArOCH_2CH_2\underline{CH_2}CH_2CH_2ONO_2Ar$).

^{13}C NMR (101 MHz, $CDCl_3$) δ 190.32, 159.66, 152.44, 145.28, 143.54, 139.58, 132.58, 131.43, 128.37, 127.11, 125.83, 122.55, 119.13, 115.12, 113.26, 110.09, 69.79, 67.76, 28.78, 28.54, 22.55.

IR $\bar{\nu}$ cm^{-1}: 2920, 2853 (aromatic CH), 2225 (C≡N), 1697 (C=O).

4-[4-[6-(3-formyl-2-nitrophenoxy)hexyloxy]phenyl]benzonitrile

T_{Cr} = 30 °C; T_{NI} = 38 °C

^{1}H NMR (400 MHz, $CDCl_3$) δ 10.03 (s, 1H, ArC=OH), 7.89 (d, *J* = 8.1 Hz, 1H), 7.65 (q, *J* = 8.5 Hz, 4H), 7.57 (d, *J* = 1.5 Hz, 1H), 7.54 – 7.46 (m, 3H), 6.98 (d, *J* = 8.8 Hz, 2H), 4.20 (t, *J* = 6.3 Hz, 2H, $ArOCH_2(CH_2)_4\underline{CH_2}ONO_2Ar$), 4.02 (t, *J* = 6.4 Hz, 2H, $ArO\underline{CH_2}(CH_2)_4CH_2ONO_2Ar$),), 1.95 – 1.79 (m, 4H $ArOCH_2\underline{CH_2}CH_2CH_2\underline{CH_2}CH_2ONO_2Ar$), 1.66 – 1.51 (m, 4H, $ArOCH_2CH_2\underline{CH_2}\underline{CH_2}CH_2CH_2ONO_2Ar$).

^{13}C NMR (101 MHz, $CDCl_3$) δ 190.37, 159.74, 152.47, 145.27, 143.52, 139.57, 132.57, 131.31, 128.34, 127.08, 125.79, 122.44, 119.14, 115.10, 113.33, 110.04, 69.87, 67.89, 29.06, 28.71, 25.67, 25.59.

IR $\bar{\nu}$ cm^{-1}: 2940, 2862 (aromatic CH), 2223 (C≡N), 1700 (C=O).

2.2.2 *[4[(E)-[4-[3-[ω-(4-cyanophenyl)phenoxy]alkyloxy]-4-nitrophenyl]methylideneamino]phenyl] 2,4-dimethoxybenzoates, 2-n series*

The **2**-*n* dimers were prepared using the method described in section *2.1.5*.

2-5

^{1}H NMR (400 MHz, $CDCl_3$) δ 8.48 (s, 1H, N=CH), 8.09 (d, *J* = 8.7 Hz, 1H, Ar), 7.91 (d, *J* = 8.2 Hz, 1H, Ar), 7.75 (s, 1H, Ar), 7.66 (q, *J* = 8.5 Hz, 4H, Ar), 7.52 (d, *J* = 8.7 Hz, 2H, Ar), 7.46 – 7.39 (m, 1H, Ar), 7.33 – 7.22 (m, 4H, Ar), 7.00 (d, *J* = 8.6 Hz, 2H, Ar), 6.61 – 6.52 (m, 2H, Ar), 4.28 (t, *J* = 6.2 Hz, 2H, $ArOCH_2(CH_2)_3\underline{CH_2}ONO_2Ar$), 4.07 (t, *J* = 6.3 Hz, 2H, $ArO\underline{CH_2}(CH_2)_3CH_2ONO_2Ar$), 3.94 (s, 3H, Ar-O$\underline{CH_3}$), 3.90 (s, 3H, Ar-O$\underline{CH_3}$), 2.04 – 1.86 (m, 4H, $ArOCH_2\underline{CH_2}CH_2\underline{CH_2}CH_2ONO_2Ar$), 1.74 (p, *J* = 7.8 Hz, 2H, $ArOCH_2CH_2\underline{CH_2}CH_2CH_2ONO_2Ar$).

^{13}C NMR (101 MHz, $CDCl_3$) δ 165.11, 163.67, 162.32, 159.70, 157.51, 152.64, 150.10, 148.17, 145.31, 141.32, 141.10, 134.53, 132.58, 131.38, 128.36, 127.11, 125.92, 122.87, 121.87, 121.41, 119.16, 115.13, 112.80, 111.01, 110.05, 104.88, 99.07, 69.61, 67.84, 56.07, 55.62, 28.81, 28.64, 22.59.

IR $\bar{\nu}$ cm^{-1}: 2942, 2860 (aromatic CH), 2222 (C≡N), 1738 (C=O).

MS (ESI+, m/z) = $[M+Na]^+$: Calculated for $C_{40}H_{35}N_3O_8Na$: 708.2322 Found: 708.2316.

2-6

^{1}H NMR (400 MHz, $CDCl_3$) δ 8.50 (s, 1H, N=CH), 8.11 (d, *J* = 8.7 Hz, 1H, Ar), 7.93 (d, *J* = 8.2 Hz, 1H, Ar), 7.77 (d, *J* = 1.5 Hz, 1H, Ar), 7.68 (d, *J* = 8.4 Hz, 4H, Ar), 7.55 (d, *J* = 8.7 Hz, 2H, Ar), 7.45 (dd, *J* = 8.3, 1.5 Hz, 1H, Ar), 7.35 – 7.25 (m, 4H, Ar), 7.02 (d, *J* = 8.5 Hz, 2H, Ar), 6.64 – 6.55 (m, 2H, Ar), 4.28 (t, *J* = 6.3 Hz, 2H, $ArOCH_2(CH_2)_4\underline{CH_2}ONO_2Ar$), 4.07 (t, *J* = 6.4 Hz, 2H, $ArO\underline{CH_2}(CH_2)_4CH_2ONO_2Ar$), 3.96 (s, 3H, Ar-O$\underline{CH_3}$), 3.93 (s, 3H, Ar-O$\underline{CH_3}$), 1.99 – 1.86 (m, 4H, $ArOCH_2\underline{CH_2}CH_2CH_2\underline{CH_2}CH_2ONO_2Ar$), 1.66 – 1.59 (m, H, $ArOCH_2CH_2\underline{CH_2}\underline{CH_2}CH_2CH_2ONO_2Ar$).

^{13}C NMR (101 MHz, $CDCl_3$) δ 165.12, 163.68, 162.32, 159.77, 157.57, 152.69, 150.09, 148.19, 145.32, 141.32, 141.07, 134.53, 132.57, 131.31, 128.35, 127.10, 125.89, 122.87, 121.86, 121.34, 119.16, 115.12, 112.80, 111.00, 110.02, 104.88, 99.07, 69.67, 67.94, 56.07, 55.62, 29.08, 28.81, 25.68, 25.63.

IR $\bar{\nu}$ cm^{-1}: 2942, 2863 (aromatic CH), 2225 (C≡N), 1736 (C=O).

MS (ESI+, m/z) = $[M+Na]^+$: Calculated for $C_{41}H_{37}N_3O_8Na$: 722.2478 Found: 722.2470.

3. Molecular models

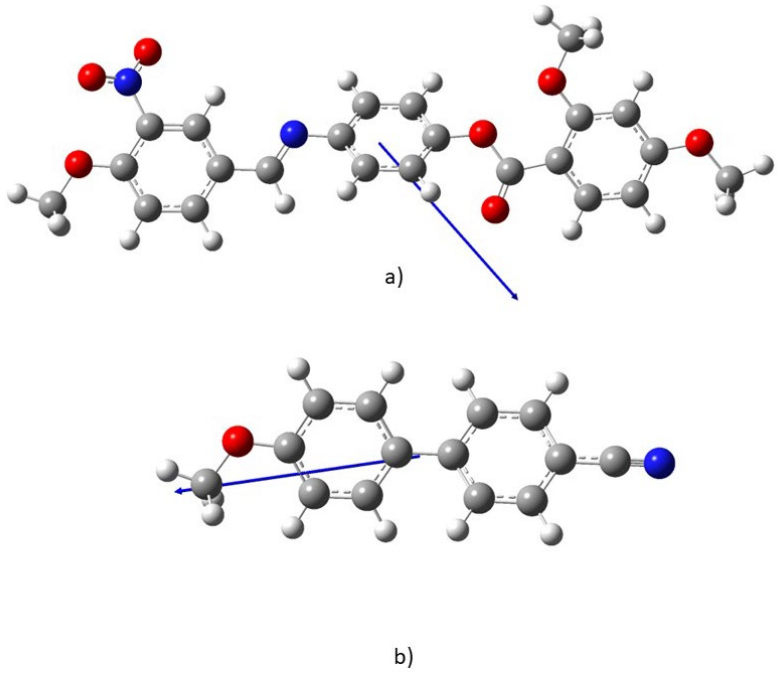

Figure ES1. Ball and stick models indicating the direction of the dipole moments of (a) [4-[(E)-(4-methoxy-3-nitrophenyl)methylideneamino]phenyl] 2,4-dimethoxybenzoate and (b) 4-methoxycyanobiphenyl.

References

1. Attard GS, Date RW, Imrie CT, Luckhurst GR, Roskilly SJ, Seddon JM, et al. Nonsymmetrical dimeric liquid-crystals - the preparation and properties of the alpha-(4-cyanobiphenyl-4'-yloxy)-omega-(4-n-alkylanilinebenzylidene-4'-o xy)alkanes. Liq Cryst. 1994;16:529-581.